Mode coupling of interaction quenched ultracold few-boson ensembles in periodically driven lattices

S. I. Mistakidis[1] and P. Schmelcher[1,2]

[1]*Zentrum für Optische Quantentechnologien, Universität Hamburg, Luruper Chaussee 149, 22761 Hamburg, Germany*

[2]*The Hamburg Centre for Ultrafast Imaging, Universität Hamburg, Luruper Chaussee 149, 22761 Hamburg, Germany*

(Received 11 April 2016; published 24 January 2017)

The out-of-equilibrium dynamics of interaction quenched finite ultracold bosonic ensembles in periodically driven one-dimensional optical lattices is investigated. It is shown that periodic driving enforces the bosons in the outer wells of the finite lattice to exhibit out-of-phase dipolelike modes, while in the central well the atomic cloud experiences a local breathing mode. The dynamical behavior is investigated with varying driving frequencies, revealing resonantlike behavior of the intrawell dynamics. An interaction quench in the periodically driven lattice gives rise to admixtures of different excitations in the outer wells, enhanced breathing in the center, and amplification of the tunneling dynamics. We then observe multiple resonances between the inter- and the intrawell dynamics at different quench amplitudes, with the position of the resonances being tunable via the driving frequency. Our results pave the way for future investigations of the use of combined driving protocols in order to excite different inter- and intrawell modes and to subsequently control them.

DOI: 10.1103/PhysRevA.95.013625

I. INTRODUCTION

Ultracold atoms in optical lattices offer an ideal platform for simulating certain problems of condensed matter physics and constitute many-body systems exhibiting a diversity of physical phenomena. In particular, the understanding of the nonequilibrium dynamics of strongly correlated many-body systems in optical lattices is currently one of the most challenging problems for both theory and experiment. This dynamics is typically triggered by an external periodic driving [1–4] or an instantaneous change (quench) of a Hamiltonian parameter [5]. Remarkable dynamical phenomena employing periodic driving [1,2] of the optical lattice include Bloch oscillations [6–8], realization of the superfluid–to–Mott insulator phase transition [9], topological states of matter [10], artificial gauge fields [11], realization of ferromagnetic domains [12,13], and even applications to quantum computation [14]. On the other hand, quench dynamics enables us to explore, among others, the light-cone effect in the spreading of correlations [15,16], the Kibble-Zurek mechanism [17,18], and the question of thermalization [19,20]. Driving or quenches can also be used in order to generate energetically low-lying collective modes, such as the dipole [21,22] or the breathing [23–27] mode. In general, a sudden displacement or a periodic shaking of the external trap induces a dipole oscillation of the atomic cloud, while a quench of the frequency of the trap excites a breathing mode of the cloud. These modes constitute a main probe both for theoretical investigations, to understand and interpret the nonequilibrium dynamics, and for experiments, as they can be used in order to measure key quantities of trapped many-body systems [23].

Recently, increasing effort has been devoted to controlling the atomic motion in optical lattices by subjecting them to time-periodic external driving [28–31] and investigating the optimal driving protocol [32–34]. In this direction, it is important to carefully explore and design the relevant driving protocol to transfer the energy to the desired final degrees of freedom. To trigger or even control a certain type of (collective) modes of the dynamics, widely used techniques in the literature constitute either periodic driving of the lattice potential, e.g., a lattice shaking, or a quench of a parameter of the system, e.g., a lattice amplitude quench or an interaction quench. In the former case a tunable local dipole mode and a resonant intrawell dynamics were recently explored by shaking an optical lattice [35]. On the other hand, in the latter case it has been shown [36] that a sudden increase in the interparticle repulsion in a nondriven lattice induces a rich interwell as well as intrawell dynamics which can be coupled and consequently mixed for certain quench amplitudes. However, for decreasing repulsive forces [37] the accessible interwell tunneling channels are far fewer compared to the excited intrawell modes, and in particular, no resonant dynamics can be observed. From the above analysis it becomes evident that a crucial ingredient for the design and further control of the dynamics is the choice of the driving protocol of the system: By using different driving schemes, different types of excited modes are induced, i.e., different energetical channels can be triggered. In this direction, an intriguing question is how a combination of periodic driving and interaction quenches can be used to steer the dynamics of the system and, as a consequence, the coupling of the interwell and intrawell modes. Such an investigation will, among other things, permit us to gain a deeper understanding of the underlying microscopic mechanisms and will allow us to activate certain energy channels by using specific driving protocols for control of the different processes.

In the spirit of the above-posed question we investigate in the present work the quantum dynamics of interaction quenched few-boson ensembles trapped in periodically driven finite optical lattices. Concerning the periodic driving, vibration of the optical lattice is employed. This scheme, in contrast to shaking, induces out-of-phase dipole modes among the outer wells and a local breathing mode in the central well of the finite lattice. We cover the dynamics of the periodically driven lattice with varying driving frequencies in the complete range from adiabatic to high-frequency driving. In particular, we observe for the intermediate-driving-frequency regime, being intractable by current state of the art analytical methods [1,2], resonantlike behavior of the intrawell dynamics. This resonance is accompanied by a rich excitation spectrum

and an enhanced interwell tunneling compared to adiabatic or high-intensity driving and it is mainly of single-particle character. Indeed, it survives upon increasing interaction, obtaining faint additional features, the most remarkable being the cotunneling of an atom pair [31,38]. To induce a correlated many-body dynamics we employ an interaction quench on top of the driven lattice, thus opening energetically higher inter-well and intrawell channels. As a consequence, the interwell tunneling is amplified even for adiabatic driving, and admixtures of excitations possessing breathinglike and dipolelike components are generated. Remarkably enough, as a function of the quench amplitude, the system experiences multiple resonances between the inter- and the intrawell dynamics. This observation indicates the high degree of controllability of the system, especially for the excited modes under such a combination of driving protocols, and it is arguably one of our central results. To the best of our knowledge, this multifold mode coupling behavior unraveled with a composite driving protocol has not been reported before. Moreover, the position of the above-mentioned resonances is tunable via the driving frequency, allowing for further control of the mode coupling in optical lattices. Finally, the realization of intensified loss of coherence caused either by the resonant driving or by a quench on top of the driving is an additional indicator of the observed phenomena. To obtain a comprehensive understanding of the microscopic properties of the strongly driven and interacting system, we focus on the few-body dynamics in small lattices (specifically, four bosons in a triple-well setup). However, we provide strong evidence that our findings apply equally to larger lattice systems and particle numbers. All calculations to solve the underlying many-body Schrödinger equation are performed by employing the multiconfiguration time-dependent Hartree method for bosons (MCTDHB) [39,40], which is especially designed to treat the out-of-equilibrium quantum dynamics of interacting bosons under time-dependent modulations.

This work is organized as follows. In Sec. II we explain our setup and introduce the multiband expansion and the basic observables that we use in order to interpret the dynamics. Section III presents the effects resulting from an interaction quench of a driven triple well for filling factors larger than unity. Section IV presents the dynamics for filling factors smaller than unity. We summarize our findings and give an outlook in Sec. V. In Appendix A the nonequilibrium dynamics induced by a driven harmonic oscillator and simultaneously an interaction quenched bosonic cloud is briefly outlined. Appendix B briefly comments on the resonant response of the driven lattice, and finally, Appendix C describes our computational method.

II. SETUP AND ANALYSIS TOOLS

In the present section we briefly report on our theoretical framework. First, we introduce the protocol of the driven optical lattice and the many-body Hamiltonian. Second, the wave-function representation in terms of a multiband expansion and some basic observables for the understanding of the inter- and intrawell modes of the dynamics are introduced.

A. Setup and Hamiltonian

To model a lattice vibration, with amplitude δ and angular frequency $\omega_D = 2\pi f_D$, a spatiotemporal sinusoidal modulation is used to generate a lattice potential of the form

$$V_{\rm br}(x;t) = V_0 \sin^2[k_x(1+\delta\sin(\omega_D t))x], \tag{1}$$

with lattice depth V_0 and wave vector $k_x = \frac{\pi}{l}$, where l denotes the distance between successive potential minima. Such a potential can be realized, e.g., via acousto-optical modulators [12], which induce a frequency difference among counterpropagating laser beams. The Hamiltonian of N identical bosons of mass M following an interaction quench protocol upon the driven one-dimensional (1D) lattice reads

$$H(x;t) = \sum_{i=1}^{N} \frac{p_i^2}{2M} + V_{\rm br}(x_i;t) + g_{\rm 1D}^{(f)} \sum_{i<j} \delta(x_i - x_j), \tag{2}$$

where $g_{\rm 1D}^{(f)} = \delta g + g_{\rm 1D}^{(\rm in)}$, with $g_{\rm 1D}^{(\rm in)}$ and $g_{\rm 1D}^{(f)}$ being the initial and final interaction strengths, respectively, and δg denotes the corresponding perturbation. The short-range interaction potential between particles located at positions x_i is modeled by a Dirac delta function. The interaction is well described by s-wave scattering and the effective 1D coupling strength [41] becomes $g_{\rm 1D} = \frac{2\hbar^2 a_0}{M a_\perp^2}\left(1 - \frac{|\zeta(1/2)|a_0}{\sqrt{2}a_\perp}\right)^{-1}$. The transversal length scale is $a_\perp = \sqrt{\frac{\hbar}{M\omega_\perp}}$, with $\omega_\perp$ the frequency of the confinement, while a_0 denotes the 3D s-wave scattering length. The interaction strength can be tuned either via a_0 with the aid of Feshbach resonances [42,43] or via the transversal confinement frequency $\omega_\perp$ [44–46].

In the following, for reasons of universality, Hamiltonian (2) is rescaled in units of the recoil energy $E_R = \frac{\hbar^2 k_x^2}{2M}$. Then the corresponding length, time, and frequency scales are given in units of k_x^{-1}, $\omega_R^{-1} = \hbar E_R^{-1}$, and ω_R, respectively. For our simulations we have used a sufficiently large lattice depth, of the order of $V_0 = 10.0E_R$, such that each well includes three localized single-particle Wannier states. The confinement of the bosons in the m-well system is imposed by the use of hard-wall boundary conditions at the appropriate position $x_\sigma = \pm\frac{m\pi}{2k_x}$. Finally, for computational convenience we set $\hbar = M = k_x = 1$ and therefore all quantities below are given in dimensionless units.

B. Wave-function representation and basic observables

To understand the microscopic properties and analyze the dynamics, the notion of noninteracting multiband Wannier number states is employed. The presently used lattice potential is deep enough for the Wannier states between different wells to have a very small overlap for not too high energetic excitation. In the case of a periodically driven potential the above description can still be valid if the driving amplitude is low enough in comparison to the lattice constant l, i.e., $\delta \ll l$, such that each localized Wannier function is assigned to a certain well and the respective band mixing is fairly small. For $\delta \gg l$ the use of a time-dependent Wannier basis is more adequate. Summarizing, for a system with N bosons, m wells, and j localized single-particle states [36,37] the expansion of

the many-body bosonic wave function reads

$$|\Psi\rangle = \sum_{\{N_i\},\{I_i\}} C_{\{N_i\};\{I_i\}} \left|N_1^{(I_1)}, N_2^{(I_2)}, \ldots, N_m^{(I_m)}\right\rangle, \tag{3}$$

where $|N_1^{(I_1)}, N_2^{(I_2)}, \ldots, N_m^{(I_m)}\rangle$ is the multiband Wannier number state, the element $N_i^{(I_i)} = |n_i^{(1)}\rangle \otimes |n_i^{(2)}\rangle \otimes \ldots \otimes |n_i^{(j)}\rangle$ denotes the number of bosons being localized in the ith well, and I_i indexes the corresponding energetic excitation order. In particular, $|n_i^{(k)}\rangle$ refers to the number of bosons which reside at the ith well and kth band, satisfying the closed subspace constraint $\sum_{i=1}^{m}\sum_{k=1}^{j} n_i^{(k)} = N$. For instance, in a setup with $N = 4$ bosons confined in a triple well, i.e., $m = 3$, which includes $k = 3$ single-particle states, the state $|1^{(0)} \otimes 1^{(1)}, 1^{(0)}, 1^{(0)}\rangle$ indicates that in every well one boson occupies the zeroth excited band, but in the left well there is one extra boson localized in the first excited band. For this setup it is also important to note that one can realize four energetic classes of number states, namely, the quadruple mode $\{|4^{(I_1)}, 0^{(I_2)}, 0^{(I_3)}\rangle + \circlearrowleft\}$ (Q), the triple mode $\{|3^{(I_1)}, 1^{(I_2)}, 0^{(I_3)}\rangle + \circlearrowleft\}$ (T), the double-pair mode $\{|2^{(I_1)}, 2^{(I_2)}, 0^{(I_3)}\rangle + \circlearrowleft\}$ (DP), and the single-pair mode $\{|2^{(I_1)}, 1^{(I_2)}, 1^{(I_3)}\rangle + \circlearrowleft\}$ (SP), where $\circlearrowleft$ stands for all corresponding permutations. It is important to note that, for later convenience, we consider only the corresponding subclass with isoenergetic states and not all members, which would also include energetically unequal number states, e.g., for the single-pair mode $\{|2^{(I_1)}, 1^{(I_2)}, 1^{(I_3)}\rangle, |1^{(I_1)}, 2^{(I_2)}, 1^{(I_3)}\rangle, |1^{(I_1)}, 1^{(I_2)}, 2^{(I_3)}\rangle\}$. Also, in the present consideration for a given set of excitation indices $\mathbf{I} = (I_1, I_2, I_3)$, the above-mentioned class of number states we are focusing on has similar on-site energies and will contribute significantly to the same eigenstates. Indexing each such class by α, we adopt the more compact notation $|q\rangle_{\alpha;\mathbf{I}}$ for characterization of the eigenstates in terms of number states, where the index q refers to the spatial occupation. For instance, $\{|q\rangle_{3;\mathbf{I}}\}$ with $\mathbf{I} = (1,0,0)$ represent the eigenstates which are dominated by the set of triple-pair states $\{|3^{(1)}, 1^{(0)}, 0^{(0)}\rangle,\ |0^{(0)}, 3^{(1)}, 1^{(0)}\rangle,\ |1^{(0)}, 0^{(0)}, 3^{(1)}\rangle,\ |1^{(0)}, 3^{(1)}, 0^{(0)}\rangle,\ |0^{(0)}, 1^{(0)}, 3^{(1)}\rangle,\ |3^{(1)}, 0^{(0)}, 1^{(0)}\rangle\}$, and the index q runs from 1 to 6.

Below, a few basic observables which refer to the inter- and intrawell generated modes are introduced and their expansion in terms of the multiband number state basis is given. Note that henceforth we denote by $|\Psi(0)\rangle = \sum_{q;\alpha;\mathbf{I}} C^{q}_{\alpha;\mathbf{I}} |q\rangle_{\alpha;\mathbf{I}}$ the initial wave function in terms of the eigenstates $|q\rangle_{\alpha;\mathbf{I}}$ of the final Hamiltonian. A time-resolved measure for the impact of the external driving on the system is provided via the fidelity $F_{\{\lambda_i\}}(t) = |\langle\Psi(0)|\Psi_{\{\lambda_i\}}(t)\rangle|^2$, which is the overlap between the time evolved and the initial (ground) state. Note the dependence of the fidelity on the set of parameters $\{\lambda_i\}$, e.g., the driving frequency ω_D, the interaction strength g, and the particle number N. The expansion of the fidelity reads

$$F_{\{\lambda_i\}}(t) = \sum_{q_1;\alpha;\mathbf{I}} \left|C^{q_1}_{\alpha;\mathbf{I}}\right|^4 + \sum_{q_1,q_2;\alpha,\beta;\mathbf{I}} \left|C^{q_1}_{\alpha;\mathbf{I}}\right|^2 \times \left|C^{q_2}_{\beta;\mathbf{I}}\right|^2 \cos\left(\epsilon^{q_1}_{\alpha;\mathbf{I}} - \epsilon^{q_2}_{\beta;\mathbf{I}}\right)t. \tag{4}$$

The second term on the right-hand side of the above expression contains the energy difference between two distinct number states and therefore offers to be a measure of the tunneling process. The indices α and β indicate a particular number-state group [36], q_i is the intrinsic index within each group, $\mathbf{I}$ corresponds to the respective energetic level, and ϵ refers to the corresponding on-site energy of a particular number state and energetic level.

For investigation of the intrawell dynamics it is appropriate to employ a local density analysis. To measure the instantaneous spreading of the cloud in the ith well we define the operator of the second moment $\sigma_i^2(t) = \langle\Psi|(x - R^{(i)}_{\mathrm{CM}})^2|\Psi\rangle$ [49]. Here $R^{(i)}_{\mathrm{CM}} = \int_{d_i}^{d_i'} dx(x - x_0^{(i)})\rho_i(x) / \int_{d_i}^{d_i'} dx\,\rho_i(x)$ refers to the coordinate of the center of mass [47,48], $x_0^{(i)}$ denotes the central point of the ith well under investigation, and d_i and d_i' correspond to the instantaneous limits of the wells, whereas $\rho_i(x)$ is the respective single-particle density. Then the expansion of the second moment for the middle well in terms of the eigenstates of the final Hamiltonian reads

$$\sigma_M^2(t) = \sum_{\alpha;q_1;\mathbf{I}} \left|C^{q_1}_{a;\mathbf{I}}\right|^2_{\alpha;\mathbf{I}} \langle q_1|\left(x - R^{(i)}_{\mathrm{CM}}\right)^2|q_1\rangle_{\alpha;\mathbf{I}} + 2\sum_{q_1\neq q_2} \mathrm{Re}\left(C^{*q_1}_{\beta;\mathbf{I}} C^{q_2}_{\alpha;\mathbf{I}}\right)_{\beta;\mathbf{I}} \langle q_1|\left(x - R^{(i)}_{\mathrm{CM}}\right)^2|q_2\rangle_{\alpha;\mathbf{I}} \times \cos\left(\omega^{q_1}_{\beta;\mathbf{I}} - \omega^{q_2}_{\alpha;\mathbf{I}}\right)t. \tag{5}$$

Finally, as a measure of the dipole motion the intrawell asymmetry $\Delta\rho_a(t) = \rho_{a,1}(t) - \rho_{a,2}(t)$ is introduced. Here, a particular well a (in a triple well $a = L, M, R$ stands for the left, middle, and right wells, respectively) is divided from the center point into two equal sections, with $\rho_{a,1}(t)$ and $\rho_{a,2}(t)$ being the respective integrated densities of the left and right parts during the evolution. The expectation value of the asymmetry operator is expressed as

$$\langle\Psi|\Delta\rho(t)|\Psi\rangle = \sum_{q_1;\alpha;\mathbf{I}} \left|C^{q_1}_{\alpha;\mathbf{I}}\right|^2_{\mathbf{I};\alpha} \langle q_1|\Delta\rho|q_1\rangle_{\alpha;\mathbf{I}} + 2\sum_{q_1\neq q_2} \mathrm{Re}\left(C^{*q_1}_{\alpha;\mathbf{I}} C^{q_2}_{\beta;\mathbf{I}}\right)_{\mathbf{I};\alpha} \langle q_1|\Delta\rho|q_2\rangle_{\beta;\mathbf{I}} \times \cos\left[\left(\omega^{q_1}_{\alpha;\mathbf{I}} - \omega^{q_2}_{\beta;\mathbf{I}}\right)t\right]. \tag{6}$$

C. First-order coherence

The spectral representation of the reduced one-body density matrix [50–52] reads

$$\rho_1(x,x';t) = \sum_{\alpha=1}^{M} n_\alpha(t)\varphi_\alpha(x,t)\varphi_\alpha^*(x',t), \tag{7}$$

where $\varphi_\alpha(x,t)$ are the so-called natural orbitals and M corresponds to the considered number of orbitals. The population eigenvalues $n_\alpha(t) \in [0,1]$ characterize the fragmentation of the system [53–55,57]: For only one macroscopically occupied orbital the system is said to be condensed; otherwise it is fragmented.

To quantify the degree of first-order coherence during the dynamics, the normalized spatial first-order correlation function $g^{(1)}(x,x';t)$ is defined:

$$g^{(1)}(x,x';t) = \frac{\rho_1(x,x';t)}{\sqrt{\rho_1(x;t)\rho_1(x';t)}}. \tag{8}$$

It is known that for $|g^{(1)}(x,x';t)|^2 < 1$ the corresponding visibility of interference fringes in an interference experiment is less than 100% and this case is referred to as loss of coherence. On the contrary, when $|g^{(1)}(x,x';t)|^2 = 1$ the fringe visibility of the interference pattern is maximal and is referred to as full coherence. The above quantity depends strongly on the various parameters of the Hamiltonian, and an investigation of the aforementioned dependence is reported in Sec. IV.

III. INTERACTION QUENCH DYNAMICS ON A DRIVEN LATTICE FOR FILLING FACTOR $\nu > 1$

To analyze the dynamics of our system, it is instructive first to comment on the relation between the ground state and its dominant interaction-dependent spatial configuration employing the multiband expansion. Let us consider a setup with four bosons in a triple well (which is our workhorse). Within the weak-interaction regime $0 < g < 0.1$ the dominant spatial configuration of the system is $|1^{(0)},2^{(0)},1^{(0)}\rangle$, while states of double-pair occupancy, e.g., $|2^{(0)},2^{(0)},0^{(0)}\rangle$, and triple-pair occupancy, e.g., $|1^{(0)},3^{(0)},0^{(0)}\rangle$, possess a small contribution. In the intermediate-interaction regime $0.1 < g < 1.0$ the system is described by a superposition of the lowest band states, which are predominantly of single-pair occupancy, e.g., $|1^{(0)},2^{(0)},1^{(0)}\rangle$, $|2^{(0)},1^{(0)},1^{(0)}\rangle$, and double-pair occupancy, e.g., $|2^{(0)},2^{(0)},0^{(0)}\rangle$, while energetically higher states than the first excited band start to be occupied. For further increasing repulsion, e.g., $1.0 < g < 5.0$, the excited states gain more population and the corresponding ground-state configuration is characterized by an admixture of ground-band (predominantly of single-pair occupancy) and excited-band (to the first and even to the second band) states.

In the following, we investigate the effect of an interaction quench upon a periodically driven finite lattice. Note that we consider interaction quenches imposed at $t = 0$ or after a short transient time. The resulting dynamics is qualitatively the same. We refer, for brevity, to the effect of an interaction quench performed at $t = 0$, i.e., when the periodic driving also starts. To be more specific, below we first explore the effect of an interaction quench for various driving frequencies and compare the induced dynamics with an unquenched system. Subsequently, the dynamics for a fixed driving frequency with varying quench amplitudes is investigated. We remark that in each case we consider quench amplitudes for which the induced above-barrier transport is suppressed.

A. Case I: Interaction quench dynamics for different driving frequencies

We explore the effect of an interaction quench on top of a periodically driven triple-well potential with four bosons in the weak-interaction regime ($g = 0.05$), where the dominant spatial configuration of the ground state corresponds to states of single-pair occupancy, e.g., $|1^{(0)},2^{(0)},1^{(0)}\rangle$. To demonstrate the difference between the dynamics of the quenched and that of the unquenched bosonic ensemble let us first investigate the response of an explicitly driven system, i.e., with $\delta g = 0$. Figure 1(a) shows $F_{\{\omega_D\}}(t)$ (see also Sec. II B) with varying ω_D. It is observed that for $0 < \omega_D < 1.5$ (nearly adiabatic driving) or very intense driving $\omega_D > 12.0$ the system remains essentially unperturbed. In between, an interesting stripe pattern occurs. To be self-contained, in the following, let us classify the frequency intervals

$$\Delta\omega_{D_1} \equiv [2.0,6.0] \quad \text{and} \quad \Delta\omega_{D_2} \equiv [7.0,11.0], \tag{9}$$

where the time-evolved state of the periodically driven system deviates significantly from the initial (ground) state. Indeed, for $\omega_D \in \Delta\omega_{D_1} \equiv [2.0,6.0]$ the minimal overlap during the dynamics drops down to 0.1, whereas for $\omega_D \in \Delta\omega_{D_2} \equiv [7.0,11.0]$ the system maximally departs from the initial state by a percentage of the order of 30%. To probe the effect of the interactions and of the driving frequency on the overall dynamics, the inset in Fig. 1(a) illustrates $\bar{F}_{\{\omega_D\}} = \int_0^T dt\, F_{\{\omega_D\}}(t)/T$ (T denotes the considered evolution time) at $\omega_D = 1.5$ and at $\omega_D = 2.75 \in \Delta\omega_{D_1}$ for different initial interactions and particle number. Focusing on the same driving frequency ω_D and a large interparticle interaction we observe that the mean response of the system decreases as a function of the particle number and therefore the system can be driven more efficiently out of equilibrium. The same observation holds for a fixed interaction strength and particle number but a driving frequency below and in the region $\Delta\omega_{D_1}$, e.g., for $N = 4$, $g = 3$, $\bar{F}_{\{\omega_D=1.5\}} = 0.9405$, while $\bar{F}_{\{\omega_D=2.75\}} = 0.1202$. Let us now inspect how an interaction quench distorts the fidelity evolution. Figure 1(b) shows $F_{\{\omega_D,\delta g\}}(t)$ for $\delta g = 2.0$ (performed at $t = 0$, i.e., simultaneously with the driving) with varying ω_D. It is observed that the combination of driving and interaction quench brings the system significantly out of equilibrium for every driving frequency. To understand the effect of the quench on the system let us compare Fig. 1(b) with Fig. 1(a) for the fidelity evolution of the driven but unquenched system. Indeed, an interaction quench introduces more energy into the system, and as a consequence the final evolving state deviates significantly from the initial one even in the region of adiabatic driving, e.g., $\omega_D = 0.5$, or high-frequency driving, e.g., $\omega_D = 14.0$, as shown in Fig. 1(b). For instance, $\bar{F}_{\{\omega_D=1.0,\delta g=0\}} = 0.98$ and $\bar{F}_{\{\omega_D=1.0,\delta g=2.0\}} = 0.81$, while $\bar{F}_{\{\omega_D=14.0,\delta g=0\}} = 0.92$ and $\bar{F}_{\{\omega_D=14.0,\delta g=2.0\}} = 0.78$. Finally, as an estimate we report that according to our simulations the deviation of $\bar{F}$ between the unquenched and the quenched system ranges from 12% to 70%.

To analyze the role of dynamical fragmentation [55,56] [see Eq. (7)], Fig. 1(c) shows the deviation from unity, $\lambda(t) = 1 - n_1(t)$, during the evolution of the first natural population for different driving frequencies ω_D and no quench. Note here that even $\lambda(0) \neq 0$, i.e., as a result of the finite repulsion the initial state possesses a small degree of fragmentation. As shown, $\lambda(t)$ is always significantly above 0, confirming the fragmentation process. Focusing on different ω_D's we note that the temporal average of the fragmentation, i.e., $\bar{\lambda} = \int dt\lambda(t)/T$, increases if $\omega_D \in \Delta\omega_{D_1} \cup \Delta\omega_{D_2}$, while for the regions where $F_{\{\omega_D\}} \simeq 1$ it decreases but never tends to a perfectly condensed state. Note also that for $\omega_D \notin \Delta\omega_{D_1} \cup \Delta\omega_{D_2}$, $\lambda(t)$ possesses low-amplitude oscillations, whereas for $\omega_D \in \Delta\omega_{D_1} \cup \Delta\omega_{D_2}$ the external driving introduces high-amplitude variations in $\lambda(t)$. As expected the interparticle repulsion supports the fragmentation process [see $\lambda(t)$ for $\omega_D = 3.0$, $g = 1.0$ and $\delta g = 0.0$ in Fig. 1(c)]. The effect of an interaction quench on the fragmentation process is

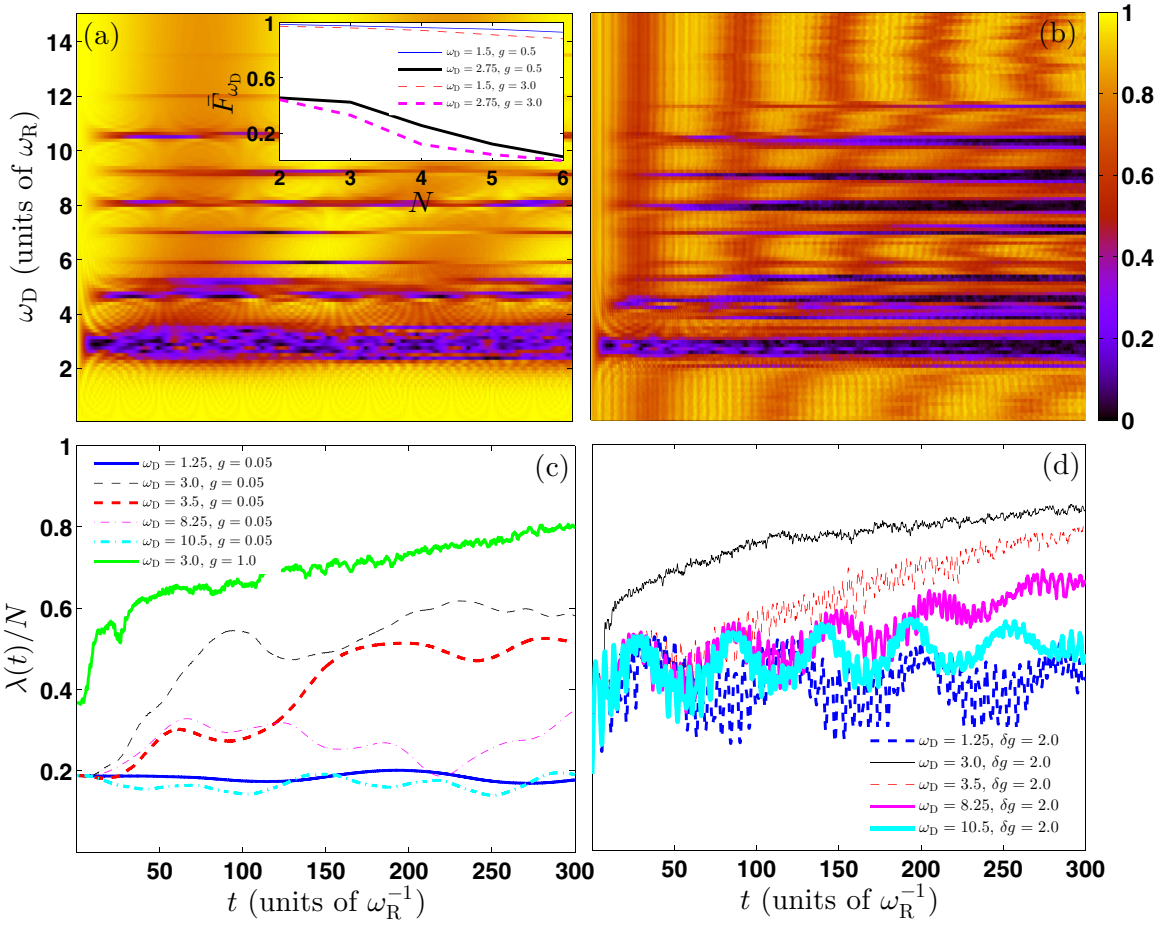

FIG. 1. (a) Time evolution of the fidelity $F_{\{\omega_D\}}(t)$ as a function of the driving frequency ω_D. The driving amplitude is $\delta = 0.03$ and the initial state corresponds to the ground state of four weakly interacting bosons with $g = 0.05$ confined in a triple well. Inset: Mean response $\bar{F}_{\{\omega_D\}}$ at $\omega_D = 0.75$ and at $\omega_D = 2.75$ for different interparticle repulsions, $g = 0.5$ and $g = 3.0$, as a function of the particle number N (see legend). (b) Same as (a), but for a fixed interaction quench, with amplitude $\delta g = 2.0$, on top of the driven triple well. (c) Deviation from unity of the first natural occupation number, i.e., $\lambda(t) = 1 - n_1(t)$, during the evolution for different driving frequencies ω_D (see legend). The effect of a stronger interparticle repulsion for $g = 1.0$ at $\omega_D = 3.0$ in the fragmentation process is also shown. (d) The same as (c), but for a fixed interaction quench, $\delta g = 2.0$, upon the driving.

shown in Fig. 1(d) employing $\lambda(t)$ for $\delta g = 2.0$ and the same driving frequencies as in Fig. 1(c). A tendency toward a higher fragmented state for every ω_D, at least for certain time periods, is manifest. Comparing $\lambda(t)$ for ω_D below $\Delta\omega_{D_1}$, in the unquenched case, we observe that the interaction quench introduces high-amplitude variations, while for $\omega_D \in \Delta\omega_{D_1} \cup \Delta\omega_{D_2}$, $\lambda(t)$ shows a monotonic increase towards a fully fragmented state. Thus, in conclusion, the fragmentation process under an interaction quench is enhanced, which is attributed to the consequent rise in the interparticle repulsion.

To identify the effect of an interaction quench on the one-body level, Fig. 2 compares $\rho_1(x,t)$ without and with an interaction quench on top of the periodically driven triple well for $\omega_D = 0.75$ and amplitude $\delta = 0.03$. Without quench, the one-body density [see Fig. 2(a)] shows a weak response, a local dipole mode in the outer wells, and a local breathing mode [hardly visible in Fig. 2(a) due to weak driving] in the central well due to the combination of the parity of the lattice (odd number of sites) and the driving scheme. The dynamics in the central well shows a compression and decompression, while the outer wells are shaken (for a lattice with an even number of sites the generated intrawell mode will be solely a local dipole mode). As shown, by performing a quench [see Fig. 2(b)] at $\delta g = 2.0$, the breathinglike mode in the central well is enhanced, while in the outer wells the cloud exhibits admixtures of excitations consisting of a dipole and a breathing component. Focusing on the dynamics of the left well it is obvious that the atomic cloud oscillates inside the well with a varying amplitude, i.e., it performs an oscillation with a simultaneous compression and decompression. Finally, the interwell tunneling mode, which is manifested as a direct population transport from the middle to the outer wells and accompanies the whole process, is amplified. To illustrate explicitly the evolution of the atomic cloud in each well we follow the $\rho_1(x,t) = 0.25$ of the local density, shown as the thick white line on top of the density. It is shown that in the central well the cloud compresses and decompresses during the evolution, while in the outer wells the cloud oscillates, also changing its width (in Appendix A, this mode is generated in a harmonic trap for a deeper understanding).

To obtain a quantitative understanding of the interwell tunneling dynamics, let us investigate the spectrum of the fidelity,

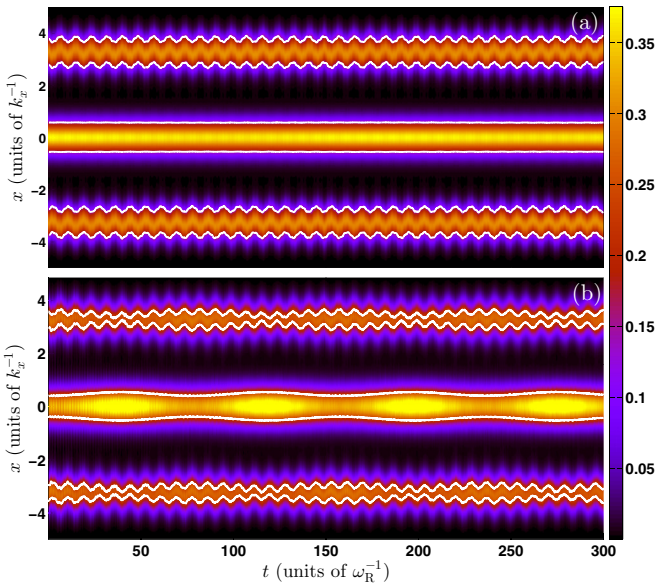

FIG. 2. Time evolution of the one-body density $\rho_1(x,t)$ caused by a periodically driven triple well with (a) $\omega_D = 0.75$ and (b) a simultaneous interaction quench with amplitude $\delta g = 2.0$. White contours, at $\rho_1(x,t) = 0.25$, are plotted on top in order to facilitate a comparison of the atomic motion between the unquenched (a) and the quenched (b) systems. The driving amplitude is fixed at the value $\delta = 0.03$ and the initial state corresponds to the ground state of four weakly interacting bosons with $g = 0.05$.

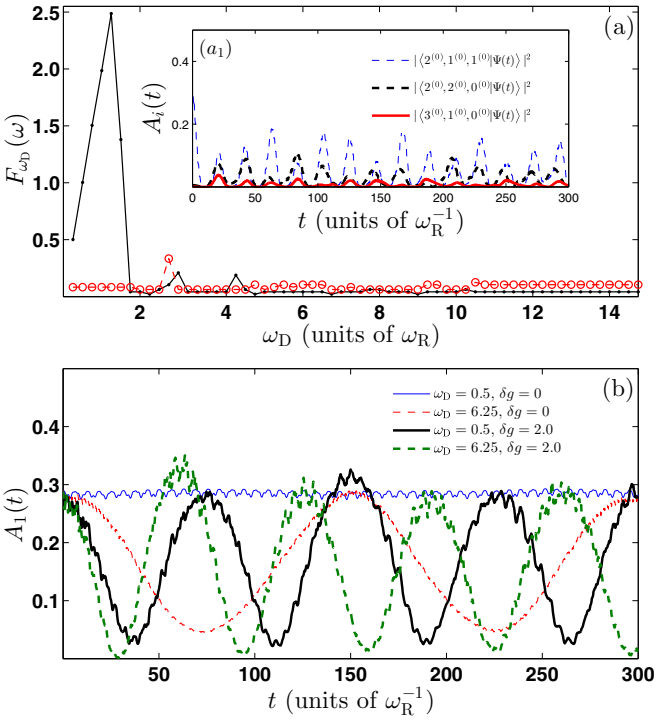

FIG. 3. (a) Spectrum of the fidelity $F_{\{\omega_D\}}(\omega)$ as a function of the driving frequency ω_D. Black dots correspond to $F_{\{\omega_D,\delta g=0.0\}}(\omega)$, i.e., to the unquenched system, while open red circles refer to $F_{\{\omega_D,\delta g=2.0\}}(\omega)$, i.e., to the case of a simultaneous interaction quench with amplitude $\delta g = 2.0$ on top of the driving. Inset (a_1): Tunneling probabilities $A_1(t)$, $A_2(t)$, and $A_3(t)$ (see text and legend) at $\omega_D = 2.75$. (b) Comparison of the single-particle tunneling probabilities $A_1(t)$ in a periodically driven triple well without and with a simultaneous interaction quench for various driving frequencies ω_D (see legend). The driving amplitude is fixed at the value $\delta = 0.03$ and the initial state corresponds to the ground state of four weakly interacting bosons with $g = 0.05$.

i.e., $F_{\{\omega_D,\delta g\}}(\omega) = \frac{1}{\pi}\int dt\, F_{\{\omega_D,\delta g\}}(t)e^{i\omega t}$ [see also Eq. (4)]. Figure 3(a) shows the tunneling spectrum of both the unquenched (see black line) and the quenched (see red line) systems with respect to the driving frequency. Indeed, employing Eq. (4) we obtain that for the unquenched system the dominant tunneling process for every ω_D corresponds to tunneling within the SP mode [e.g., between state $|2^{(0)},1^{(0)},1^{(0)}\rangle$ and state $|1^{(0)},2^{(0)},1^{(0)}\rangle$]. It is important here to note that for $\omega_D \in \Delta\omega_{D_1}$ additional tunneling modes from the SP to the DP mode [e.g., from $|1^{(0)},2^{(0)},1^{(0)}\rangle$ to $|2^{(0)},2^{(0)},0^{(0)}\rangle$] and from the SP to the T mode [e.g., from $|1^{(0)},2^{(0)},1^{(0)}\rangle$ to $|3^{(0)},1^{(0)},0^{(0)}\rangle$] can be generated. To illustrate this fact we depict in the inset in Fig. 3(a) the probabilities $A_1(t) = |\langle 2^{(0)},1^{(0)},1^{(0)}|\Psi(t)\rangle|^2$, $A_2(t) = |\langle 2^{(0)},2^{(0)},0^{(0)}|\Psi(t)\rangle|^2$, and $A_3(t) = |\langle 3^{(0)},1^{(0)},0^{(0)}|\Psi(t)\rangle|^2$ at $\omega_D = 2.75$. It is shown that $A_2(t)$ and $A_3(t)$, although suppressed in comparison to $A_1(t)$, possess significant populations. We remark here that a similar tunneling procedure corresponding to atom-pair tunneling has been observed for few atoms confined in a driven double well in Ref. [31]. However, for the quenched system the tunneling takes place only within the SP mode, while the remaining tunneling modes are supressed, due to the quench, even for $\omega_D \in \Delta\omega_{D_1}$. To illustrate the effect on the tunneling dynamics of an interaction quench upon the driven lattice, Fig. 3(b) shows the probability $A_1(t)$ for both the unquenched and the quenched system for various driving frequencies. As shown the effect of the quench depends on the driving frequency. Indeed, for $\omega_D \leqslant \min(\Delta\omega_{D1})$ the quench decreases the frequency of the tunneling branch [see the open red circles in Fig. 3(a), which correspond to the interaction quenched fidelity spectrum] and leads to a significant enhancement of the amplitude of this tunneling branch [e.g., see the blue and black lines in Fig. 3(b)]. The latter is a consequence of the fact that the interaction quench injects energy into the system. However, for $\omega_D > \max(\Delta\omega_{D1})$ the tunneling branch is quite insensitive to the quench because both the frequency and the amplitude of the tunneling probability are slightly higher [see Figs. 3(a) and 3(b)].

To determine the frequencies of the local dipole mode in the outer wells we calculate the spectrum $\Delta\rho_L(\omega) = \frac{1}{\pi}\int dt\,\Delta\rho_L(t)e^{i\omega t}$. The analysis of the corresponding breathing component is performed in the next subsection, where we examine in more detail the effects of the quench dynamics. Figure 4(a) presents $\Delta\rho_L(\omega)$, where two emergent frequency branches [denoted (a_1) and (a_2) in the spectrum] of the intrawell oscillations are visible. It is observed that for driving frequencies $\omega_D \in [0,0.5]$ the intrawell dipole mode possesses two distinct frequencies which come into resonance in the region $\omega_D \in [2,3]$ and then, for $\omega_D > 3.0$, are again well separated. To gain insight into the impact of an interaction quench, performed on top of the driving, on the intrawell density oscillations, Fig. 4(b) shows $\Delta\rho_L(t)$ at resonance

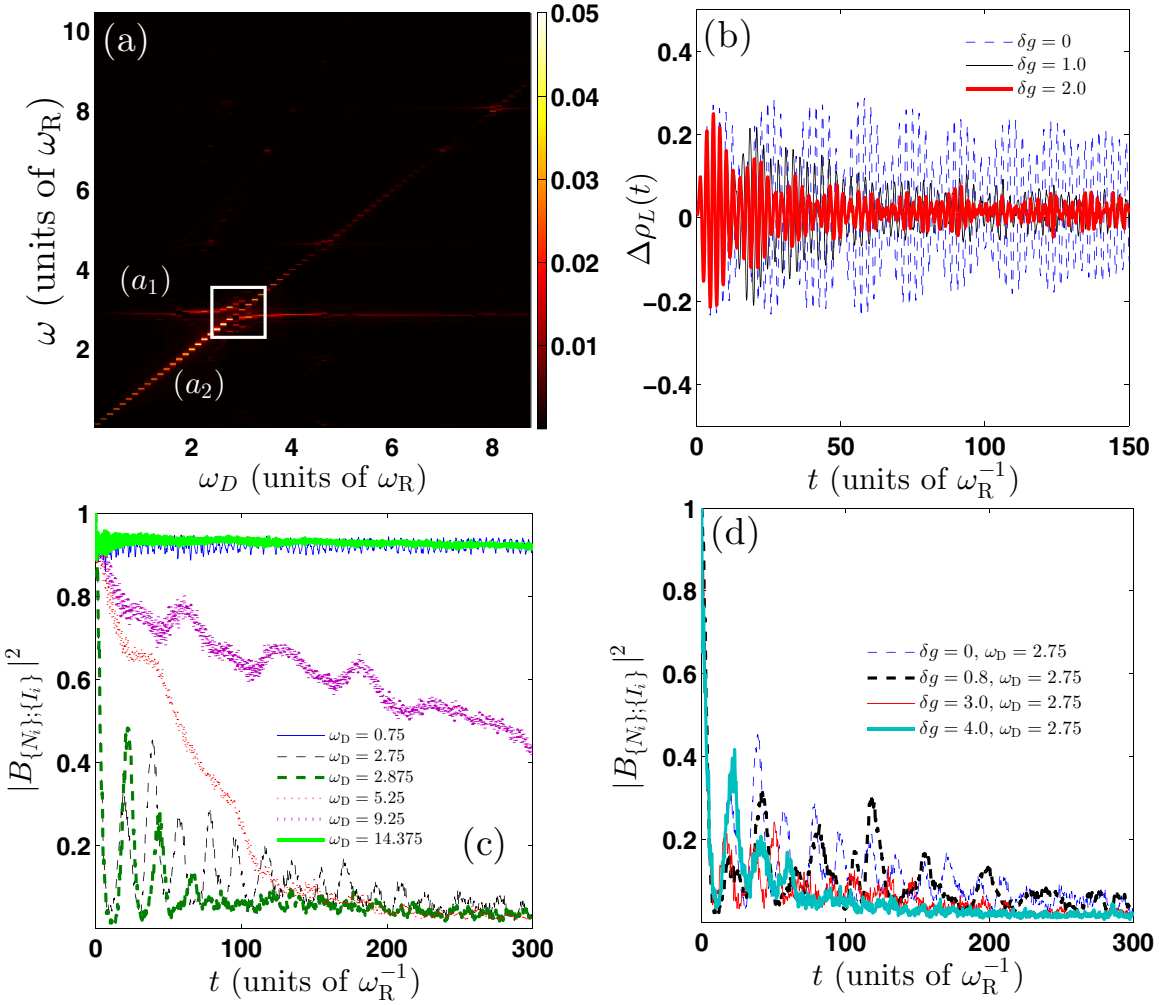

FIG. 4. (a) Spectrum of the intrawell asymmetry for the left well $\Delta\rho_L(\omega)$ in a driven triple well, with respect to the driving frequency ω_D. The white rectangle indicates the region of resonance. (b) Intrawell asymmetry evolution $\Delta\rho_L(t)$ at resonance ($\omega_D = 2.875$) employing different interaction quenches (see legend). (c) Excitation probability $|B_{\{N_i\};\{I_i\}}|^2$ (see text) during the evolution for different driving frequencies ω_D. (d) The same as (c), at $\omega_D = 2.75$, for different quenches on the interparticle repulsion (see legend). The driving amplitude is fixed at the value $\delta = 0.03$, while the initial state corresponds to the ground state of four weakly interacting bosons with $g = 0.05$.

($\omega_D = 2.875$) for different quench amplitudes, namely, at $\delta g = 0.0$, 1.0, and 2.0. As expected (resonance) $\Delta\rho_L(t)$ features a beating dynamics but with an increasingly decaying envelope with increasing quench amplitude, which is a direct effect of the interactions. A similar dephasing behavior holds for the other ω_D's, where $\Delta\rho_L(t)$ does not exhibit a beating pattern. Concerning the width of the resonant region different amplitudes of the interaction quench lead to a slight broadening of the resonant region. According to our calculations for the case with $\delta g = 0$ the resonant frequency region corresponds to $\omega_D \in [2,3]$, while for $\delta g = 1.0$ and $\delta g = 2.0$ the corresponding regions are $\omega_D \in [1.8,3.2]$ and $\omega_D \in [1.5,3.5]$, respectively. Summarizing, one can induce this resonant intrawell dynamics by adjusting the driving frequency and by applying an interaction quench to increase the width of the resonance and manipulate the amplitude of the intrawell oscillations.

From another perspective the above-mentioned resonant behavior can be illustrated by employing the occupation of the zeroth band of the triple well during evolution. The probability of finding all four bosons within the zeroth band (employing the multiband expansion) reads

$$\left|B_{\{N_i\};\{I_i\}}(t)\right|^2 = \sum_{\{I_i\}} \left|\left\langle N_1^{(I_1)}, N_2^{(I_2)}, N_3^{(I_3)} \middle| \Psi(t) \right\rangle\right|^2, \qquad (10)$$

where the summation is performed over the excitation indices with the imposed constraints $\sum_{i=1}^{3} n_i^{(1)} = N$ and $\sum_{i=1}^{3}\sum_{j=2}^{3} n_i^{(j)} = 0$ [see also Eq. (3)]. Figure 4(c) shows the probability $|B_{\{N_i\};\{I_i\}}(t)|^2$ of all the bosons residing in the zeroth band for various driving frequencies ω_D and a fixed amplitude $\delta = 0.03$. At resonance a complete depopulation of the zeroth band at some specific time intervals is observed. To be more precise, this probability exhibits a revival-like behavior on short time scales and decays as time evolves [see, in particular, the dashed black curve in Fig. 4(c)]. The local minima of $|B_{\{N_i\};\{I_i\}}(t)|^2$ are connected to the enhancement of the amplitude of the oscillations of the single-particle density (see also Appendix B). On the other hand, for driving frequencies away from $\Delta\omega_{D_1}$ the respective probability that

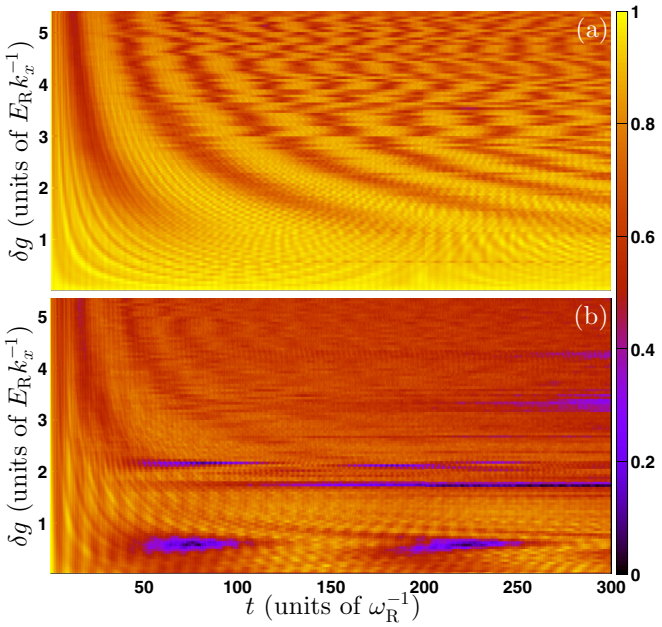

FIG. 5. Time evolution of the fidelity $F_{\{\omega_D,\delta g\}}(t)$ in a periodically driven triple well with (a) $\omega_D = 0.75$ and (b) $\omega_D = 2.75$ as a function of the quench amplitude. The driving amplitude is $\delta = 0.03$, while the initial state corresponds to the ground state of four weakly interacting bosons with $g = 0.05$.

all the bosons will occupy the zeroth band is rather high and is indeed dominant. However, significant contributions, e.g., at $\omega_D = 5.25$ or $\omega_D = 9.25$ [see Fig. 4(c)] from excited configurations cannot be neglected, especially in the regions $\Delta\omega_{D_1}$ and $\Delta\omega_{D_2}$, where the system departs from the initial state [see also Fig. 1(a)] in a prominent way. Finally, in order to explore the impact of the interaction quench at resonance, Fig. 4(d) shows $|B_{\{N_i\};\{I_i\}}(t)|^2$ for different quench amplitudes at $\omega_D = 2.75$. It is observed that for larger interaction quenches, this probability exhibits a more strongly decaying envelope, which is a pure effect of the interactions. As shown, for increasing quench amplitude the probability that the system will remain in the zeroth band, in the course of the dynamics, decays on increasingly shorter time scales and the system is dominated by different types of excitations, e.g., two, three, or four particles distributed in the first and second excited bands, as expected intuitively.

B. Case II: Periodically driven dynamics for different interaction quench amplitudes

In the following, we examine the impact of the quench amplitude δg, focusing on two driving frequency regions, i.e., for an almost-adiabatic periodic driving and in the vicinity of the resonance [see also Fig. 1(a)]. To obtain an overview of the dynamical response, Figs. 5(a) and 5(b) show the fidelity evolution with respect to δg, for fixed driving frequencies $\omega_D = 0.75$ and $\omega_D = 2.75$, respectively. As expected, for higher quench amplitudes the time-evolved final state deviates from the initial (ground) state in a prominent way. For instance, $\bar{F}_{\{\omega_D=0.75,\delta g=0\}} = 0.95$ and $\bar{F}_{\{\omega_D=0.75,\delta g=4.0\}} = 0.6$, while $\bar{F}_{\{\omega_D=2.75,\delta g=0\}} = 0.7$ and $\bar{F}_{\{\omega_D=2.75,\delta g=4.0\}} = 0.4$. Next,

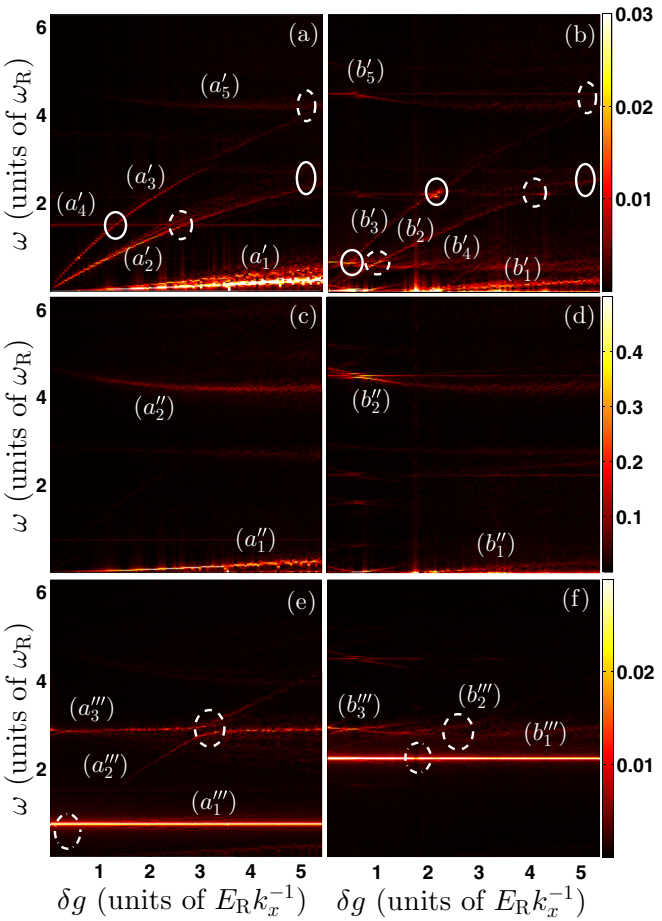

FIG. 6. The following are shown as a function of the quench amplitude δg: the fidelity spectrum $F_{\{\omega_D,\delta g\}}(\omega)$ for (a) $\omega_D = 0.75$ and (b) $\omega_D = 2.75$; the spectrum of the local-breathing mode $[\sigma_M^2(\omega)]$ for the middle well of a periodically driven triple well with (c) $\omega_D = 0.75$ and (d) $\omega_D = 2.75$; and the spectrum of the local-dipole mode $[\Delta\rho_L(\omega)]$ for the left well of a driven triple well with (e) $\omega_D = 0.75$ and (f) $\omega_D = 2.75$. Solid and dashed ellipses indicate the positions of the resonances between the tunneling and the breathing or dipole branches (see text). The driving amplitude is $\delta = 0.03$, while the initial state corresponds to the ground state of four weakly interacting bosons with $g = 0.05$.

let us proceed with a more detailed analysis in order to probe the effect of an interaction quench on the interwell tunneling dynamics and the intrawell excited modes.

To examine the tunneling dynamics, Fig. 6(a) presents the fidelity spectrum $F_{\{\delta g\}}(\omega) = \frac{1}{\pi}\int dt F_{\{\delta g\}}(t)$ as a function of the quench amplitude. Three interwell tunneling branches $(a_1' - a_3')$ can be identified. The lowest branch (a_1'), which dominates for strong quench amplitudes, refers to the energy difference $\Delta\epsilon$ within the energetically lowest-band states of the SP mode, e.g., from the initial state $|1^{(0)},2^{(0)},1^{(0)}\rangle$ to a final state $|2^{(0)},1^{(0)},1^{(0)}\rangle$. The second branch (a_2') corresponds to tunneling between the SP and the DP modes, e.g., from $|1^{(0)},2^{(0)},1^{(0)}\rangle$ to $|2^{(0)},2^{(0)},0^{(0)}\rangle$. The third branch (a_3') refers to a tunneling process among the SP and T modes, e.g., from $|1^{(0)},2^{(0)},1^{(0)}\rangle$ to $|3^{(0)},1^{(0)},0^{(0)}\rangle$. The remaining interwell tunneling branches, which correspond to transitions of

energetically higher different modes, are negligible in comparison to the aforementioned, and therefore we can hardly identify them in Fig. 6(a). To probe the effect of the driving frequency on the tunneling spectrum, Fig. 6(b) shows $F_{\{\delta g\}}(\omega)$ at $\omega_D = 2.75$ (i.e., at resonance of an explicitly driven triple well) with varying quench amplitude. The three observed tunneling branches ($b_1' - b_3'$) refer to the same transitions, i.e., between the same number states as addressed above, but they are slightly shifted to higher frequencies as a consequence of the higher driving frequency. The remaining branches, e.g., a_4' and b_4', that are visible in the spectrum, which show more prominent deviations for the different driving frequencies, correspond to other modes and interband transitions and are explained below.

To identify the frequencies of the local breathing mode we resort to the second moment $\sigma_i^2(\omega) = \frac{1}{\pi}\int dt \sigma_i^2(t) e^{i\omega t}$ for each well [see Sec. II B and Eq. (5)]. Focusing on the left well, which possesses a breathing component [see also Fig. 2(b)] we calculate the frequency spectrum of $\sigma_L^2(\omega)$, which matches the branch a_4' in the fidelity spectrum [see Fig. 6(a)]. Most importantly this frequency branch resonates with two distinct tunneling branches at different quench amplitudes, namely, at $\delta g \approx 1.0$ with branch a_3' [see the ellipse in Fig. 6(a)] and at $\delta g \approx 2.8$ with branch a_2' [see the dashed ellipse in Fig. 6(a)] of the tunneling. Turning to the middle well, Fig. 6(c) presents $\sigma_M^2(\omega)$, thus showing two main peaks (a_1''-a_2'') with respect to the quench amplitude. The lowest of these peaks refers to a tunneling mode [see also Fig. 6(a)] identified from the energy difference within the energetically lowest states of the SP mode. The appearance of this peak in the spectrum is due to the fact that the tunneling can induce a modulation of the width of the local wave packet. The second peak, located at $\omega_2 \approx 4.5$, refers to an interband process, i.e., to a transition from $|1^{(0)},2^{(0)},1^{(0)}\rangle$ to $|1^{(0)},1^{(0)} \otimes 1^{(2)},1^{(0)}\rangle$. Inspecting now more carefully the fidelity spectrum in Fig. 6(a) we observe that the latter breathing frequency branch a_2'' [denoted a_5' in Fig. 6(a)] comes into resonance with the highest-tunneling-frequency branch (a_3') at high quench amplitudes $\delta g \approx 5.2$. However, this tunneling branch is not visible in Fig. 6(c) due to its low amplitude in comparison to the breathing (a_2'') branch. To comment on the dependence of the breathing peak (a_2'') on the interaction quench we observe that it is more sensitive to δg for $0.0 < g_f < 2.5$; otherwise it is approximately constant. To probe the effect of the driving frequency on the breathing branch of the middle well, Fig. 6(d) illustrates the spectrum of $\sigma_M^2(\omega)$ with respect to a varying δg for $\omega_D = 2.75$. The respective breathing branches, denoted b_1'' and b_2'' in the figure, are slightly disturbed in comparison to the case with $\omega_D = 0.75$. Concerning the first one, we have commented on its deviation in our discussion of Figs. 6(a) and 6(b). Focusing now on the highest-frequency branch of the breathing a significant alteration is observed: for low quench amplitudes, $0.0 < \delta g < 0.8$, it possesses a single frequency, while for $\delta g > 0.8$ the branch splits into two, with slightly different frequencies. The first is near the corresponding frequency for $\omega_D = 0.75$ but slightly larger, while the second is larger than both. Finally, let us quantitatively examine the dipole component in the outer wells by employing the frequency spectrum $\Delta\rho_L(\omega) = \frac{1}{\pi}\int dt \Delta\rho_L(t) e^{i\omega t}$ for various quench amplitudes. Figure 6(e) shows $\Delta\rho_L(\omega)$, where we can identify three dominant peaks (denoted $a_1''' - a_3'''$), which are located at $\omega_1''' \approx 1.2$, $\omega_3''' \approx 2.5$, while ω_2''' is quench dependent. The steady frequency branches (a_1''' and a_3''') correspond to the dipole mode and refer to interband transitions, e.g., from $|1^{(0)},2^{(0)},1^{(0)}\rangle$ to $|1^{(0)} \otimes 1^{(1)},1^{(0)},1^{(0)}\rangle$ or to $|1^{(0)} \otimes 1^{(2)},1^{(0)},1^{(0)}\rangle$, respectively. On the other hand, the quench-dependent frequency peak (a_2''') is related to the third interwell tunneling mode [denoted a_3' in Fig. 6(a)]. As shown in Fig. 6(e) the latter branch a_2''' experiences two resonances with each dipole branch at different quench amplitudes, namely, at $\delta g \approx 0.7$ with the lowest-frequency dipole branch (a_1''') and at $\delta g \approx 3.0$ with the higher-frequency dipole branch a_3'''. Moreover, upon examining the fidelity spectrum once again [Fig. 6(a)] more carefully, it is observed that the highest-frequency dipole branch experiences a resonance with the second interwell tunneling mode (a_2') at $\delta g \approx 5.0$. In order to reach a conclusion on the dependence of the dipole branches on the driving frequency we show in Fig. 6(f) the $\Delta\rho_L(\omega)$ at $\omega_D = 2.75$. As shown the lower-frequency dipole branch (a_1''') is strongly dependent on the driving frequency [see branch b_1''' in Fig. 6(f)], while the higher-frequency branch (a_3''') is essentially unaffected. Most importantly, the aforementioned resonant behavior still exists for $\omega_D = 2.75$ but in this case two more resonances appear in the spectrum [see Fig. 6(b)] due to a shift of the lowest-frequency dipole branch. These resonances are located at $\delta g \approx 2.1$ and $\delta g \approx 4.0$ and refer to a coupling among the second (b_2') and third (b_3') tunneling branches with the lowest-frequency dipole branch.

In the next section, we proceed to the investigation of a system with filling $\nu < 1$ in order to generalize our findings. In particular, by considering a setup with 11 wells and five particles we demonstrate that the above-discussed resonant behavior for the intrawell dynamics induced by an explicitly driven potential is present also here. Subsequently, we explore the impact of an interaction quench.

IV. QUENCH DYNAMICS IN THE DRIVEN LATTICE FOR FILLING FACTOR $\nu < 1$

Here we concentrate on a larger lattice system characterized by a filling factor smaller than unity, namely, we consider the case of five bosons trapped in an 11-well potential. To understand and interpret the dynamics let us first briefly comment on the ground-state properties of the system. An important property of the ground state is the spatial redistribution of the atoms as the interparticle repulsion increases. The noninteracting ground state ($g = 0$) is the product of the single-particle eigenstates spreading across the entire lattice, while the presence of the hard-wall boundaries renders the neighborhood of the central well of the potential slightly more populated. Increasing the repulsion within the weak-interaction regime the atoms are pushed to the outer sites, which gain and lose population in the course of increasing g [58].

In the following, let us first focus on the driven bosonic dynamics induced, at $t = 0$, by a vibrating 11-well potential to the ground state of five repulsively interacting bosons with $g = 0.05$. Figures 7(a) and 7(b) demonstrate the response of the system at the one-body level for different driving frequencies ω_D, but the same driving amplitude $\delta = 0.03$.

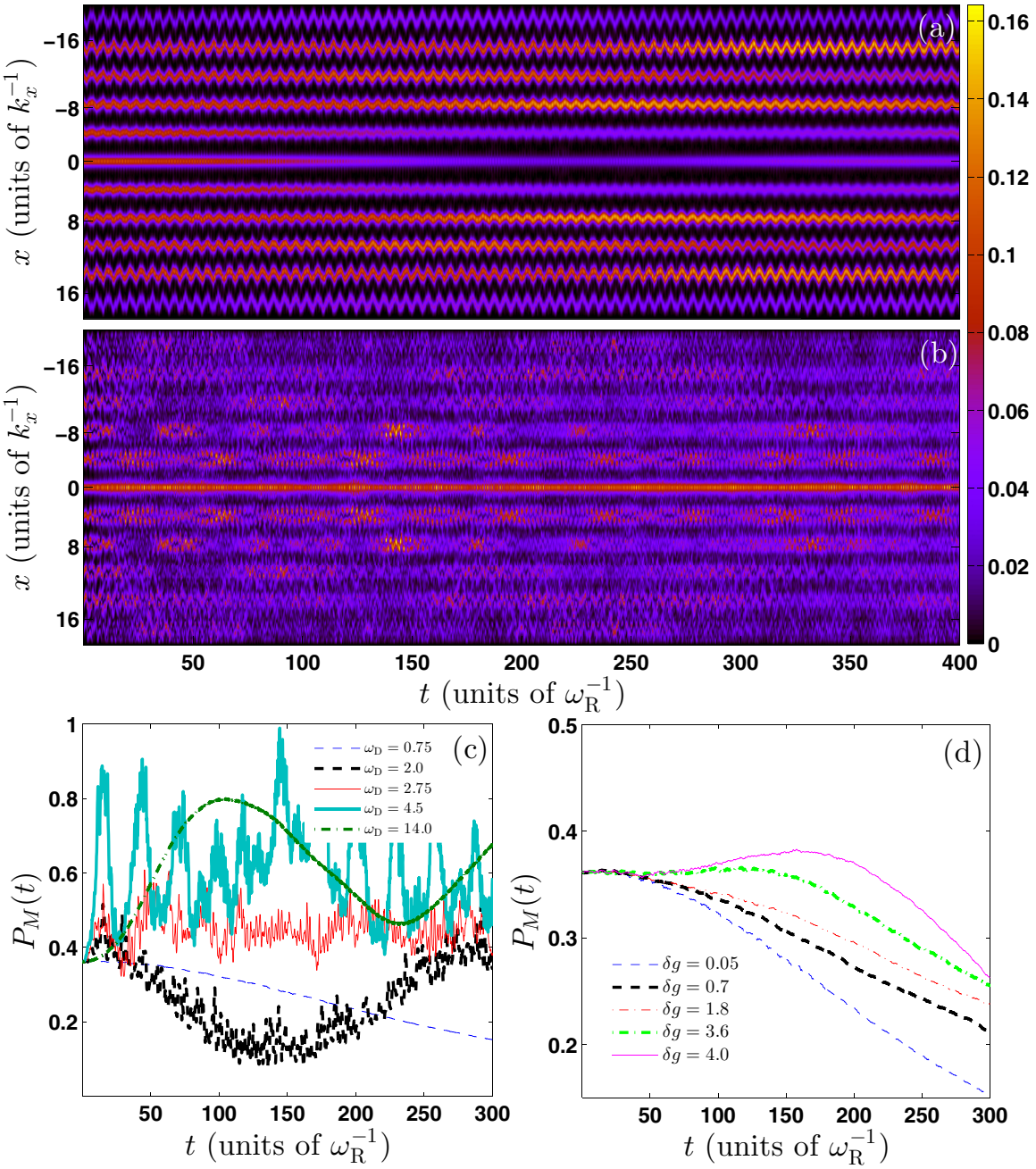

FIG. 7. Time evolution of the one-body density $\rho_1(x,t)$ in a periodically driven 11-well potential for different driving frequencies: (a) $\omega_D = 1.25$ and (b) $\omega_D = 2.875$. The driving amplitude is fixed at the value $\delta = 0.03$, while the initial state corresponds to the ground state of five weakly interacting bosons with $g = 0.05$. (c) Probability of finding all the bosons in the central well $[P_M(t)]$ during the evolution for different driving frequencies ω_D (see legend). (d) The same as (c), but for $\omega_D = 0.75$ and different quench amplitudes δg (see legend).

The overall out-of-equilibrium behavior shows characteristics to those in the case of the triple well, i.e., the occurrence of out-of-phase dipolelike modes among the outer wells of the lattice, a local-breathing mode in the central well, and an interwell tunneling mode accompanying the dynamics. In addition, a transition from nonresonant [Fig. 7(a)] to a resonant intrawell dynamics [Fig. 7(b)] upon adjusting ω_D is observed at the same frequency, $\omega_D = 2.875$, as in the triple-well case. This resonant behavior is again manifested [Fig. 7(b)] in the one-body density evolution as the formation of enhanced density oscillations at each site, being further related to a gradual depopulation of the zeroth band during evolution. In terms of the significant contributing number states we can infer that out of resonance the dynamics can well be described by the set of lowest-band states (with a small contribution from the excited-band states), while at resonance the inclusion of number states which obey the constraints $\sum_{i=1}^{11} n_i^{(1)} = N - 1$, $n_i^{(3)} = 0$, and $n_i^{(2)} = 1$ for $k = 1, \ldots, 11$ is necessary. Contributions from excited states to the second band, i.e., $\sum_{i=1}^{11} n_i^{(1)} = N - 1$, $n_i^{(2)} = 0$, and $n_i^{(3)} = 1$ for $k = 1, \ldots, 11$ also exist, but they are negligible in comparison to the excitations of the first excited band.

Another important observation here is that upon tuning the driving frequency ω_D close to resonance the tunneling dynamics is modified. To explicate the latter, we employ, as a measure of the interwell tunneling, the spatially integrated middle-well density $P_M(t) = \int_{-\pi/2}^{\pi/2} dx \rho_1(x,t)$, shown in Fig. 7(c) for different driving frequencies, namely, before, exactly at, and after the resonance. Approaching $\omega_D = 2.875$ from below, diffusion to the outer wells is observed. In the region of $\omega_D = 2.875$ the tunneling dynamics is slowed down, i.e., the occupation of the middle well fluctuates around a mean value. For $\omega_D > 2.875$ the tunneling process is modified and a tendency for the particles to concentrate in the central well is observed. Employing a corresponding number-state analysis we can infer that for $\omega_D > 2.875$, states with a higher occupancy in the central well gain prominence. The same behavior of the tunneling dynamics (before and after the resonance) is also observed in the triple-well case. Furthermore, let us inspect the influence of an interaction quench on top of the driven lattice. As expected intuitively, with increasing interaction quench the tunneling process decreases. Figure 7(d) shows $P_M(t)$ for different interaction quench amplitudes on top of the periodically driven lattice with $\omega_D = 0.75$ (i.e., away from resonance). It is observed that $P_M(t)$ becomes steady for increasingly longer times as we increase δg, thus indicating a decrease in the corresponding interwell tunneling dynamics. Finally, note that due to the low filling the admixing modes, induced after an interaction quench on the periodically driven lattice, in the outer wells are hardly visible and therefore not shown here.

Let us further investigate the signature of the resonant regions as well as the effect of the interaction quench on top of the periodically driven lattice by exploring the first-order correlation function [see Eq. (8)], in coordinate space, which quantifies the degree of spatial coherence of the interacting system [51]. It is important to stress that, within the single-orbital Gross-Pitaevskii theory, the quantum wave packet remains coherent at all times, in contrast to a many-body calculation, where it exhibits prominent time-varying structures which in turn indicate the rise of fragmentation in the system as the correlations between particles increase. From this point of view we expect a strong influence on the change in the spatial distribution of the atoms in the lattice either due to the resonant driving or as a consequence of the interaction quench. Focusing on low driving frequencies ($\omega_D = 0.75$) within the weakly interacting regime ($g = 0.05$) we observe spread of the coherence [Figs. 8(a)–8(d)] through the lattice sites as time evolves. The diagonal elements are always perfectly coherent and their first neighbors remain close to unity throughout the time evolution. The off-diagonal elements are partially coherent and oscillate around the value 0.5, while for comparatively long evolution times a site-selective, off-diagonal, long-range order appears [see Fig. 8(d)]. Turning our attention to the resonant driving [see Figs. 8(e)–8(h)] a different behavior throughout the time evolution is observed: On short time scales, only the diagonal elements remain coherent and the off-diagonal is partially coherent. As time evolves, a substantial loss of coherence is observed even on the diagonal, while the off-diagonal elements exhibit a much more prominent and complex structure. A direct comparison at equal times of the correlation functions for nonresonant and resonant

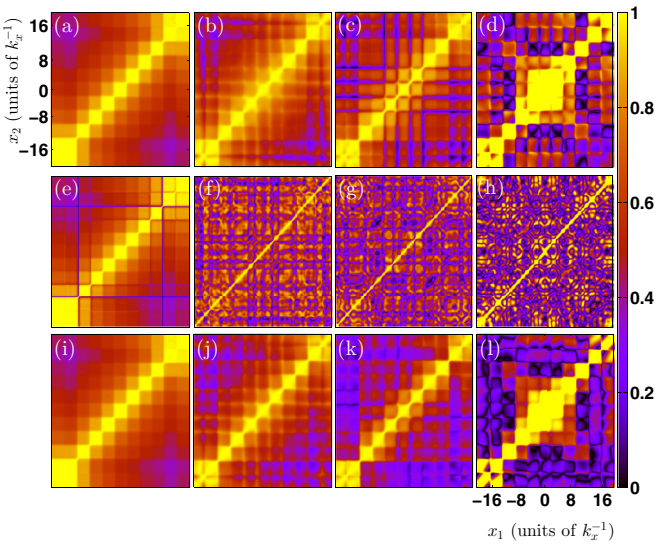

FIG. 8. One-body coherence function at different instants in time ($t_1 = 1.0$, $t_2 = 56.0$, $t_3 = 123.0$, and $t_4 = 193.0$) during the evolution caused by a periodically driven 11-well potential with (a)–(d) $\omega_D = 0.75$ and (e)–(h) $\omega_D = 3.0$. (i)–(l) Evolution of the one-body coherence in a periodically driven potential with $\omega_D = 0.75$ and a simultaneous interaction quench with amplitude $\delta g = 1.0$. The driving amplitude is fixed at the value $\delta = 0.03$ and the initial state corresponds to the ground state of five weakly interacting bosons with $g = 0.05$.

driving shows that resonant driving and loss of coherence go hand in hand. On the other hand, by performing an interaction quench on top of the driving, the coherence [see Figs. 8(i)–8(l)] is unity along the diagonal, while for sufficiently long evolution times it tends to vanish away from the diagonal. Finally, note that the off-diagonal contributions tend to fade out (but never vanish completely, even for stronger quenches, since the particles always remain delocalized) with increasing quench amplitude and a tendency toward concentration close to the diagonal is observed at equal times. This indicates that the strength of the interaction between particles strongly affects the correlations; the stronger the interparticle repulsion, the stronger the loss of coherence. As a concluding remark we can infer that either the resonant driving or a quench on top of the driving entails an intensified loss of coherence.

V. CONCLUSIONS AND OUTLOOK

In the present work, the few-body correlated nonequilibrium quantum dynamics of an interaction quenched bosonic cloud in an external periodically driven finite-size optical lattice has been investigated. The effect of an interaction quench on top of the driven lattice has been analyzed. We focus on large lattice depths and low driving amplitudes in order to limit the degree of excitations that could lead to the creation of cradle motion [37] or even to heating processes. Starting from the ground state of a weakly interacting small atomic ensemble, we examine in detail the time evolution of the system in a periodically driven optical lattice by a simultaneous interaction quench.

It has been shown that for the case of the periodically driven lattice one can induce out-of-phase local dipole modes in the

outer wells, while a local breathing mode can be generated in the central well. This is in direct contrast with the shaken lattice, where only in-phase dipole modes are excited. A wide range of driving frequencies has been considered in order to unravel the range from adiabatic to high-frequency driving. We observe that within the intermediate-frequency regimes, being intractable by current analytical methods, the system can be driven to a far out-of-equilibrium state compared to other driving-frequency regions. In particular, resonance of the intrawell dynamics occurs with enhanced tunneling dynamics, thus opening energetically higher-lying interwell tunneling channels. A prominent signature of the resonant regions as well as the effect of the interaction is provided via the study of the time dependence of the first-order coherence, where intensified loss of coherence is observed. This loss of coherence constitutes an independent signature of the resonant regions, allowing us to study it from another perspective and, potentially, to measure it in experiments. Following an interaction quench on top of the periodically driven lattice for various driving frequencies, we can trigger more effectively the interwell as well as the intrawell dynamics and steer the system towards strongly out-of-equilibrium regimes. Here, the tunneling as well as the local breathing mode in the middle well is amplified, while in the outer wells the atomic cloud experiences an admixture of a dipole and a breathing component. This admixture leads to simultaneous oscillations around the minimum of the well as well as a contraction and expansion in the course of the dynamics. Our analysis shows that one can use the interaction quench to manipulate the tunneling frequency, rendering single-particle tunneling dominant even at resonance. Concerning the on-site modes it is shown that an interaction quench can be used in order to manipulate their amplitude oscillations, yielding also a strong influence on the excitation dynamics.

Subsequently, the dynamics of the periodically driven lattice (i.e., for a fixed driving frequency) as a function of the quench amplitude has been studied. In particular, the tunneling contains three modes, the breathing possesses two frequency branches, and the corresponding admixture three branches: one from the breathing component and two which refer to the dipole component. Furthermore, five resonances between the interwell tunneling dynamics and the intrawell dynamics have been revealed. The interwell tunneling experiences a resonance with the breathing component of the central well, two resonances with the breathing component of the outer wells, and two resonances with the dipole component of the outer wells. These resonances can further be manipulated via the frequency of the periodic driving. As a result, the combination of different driving protocols can excite different inter- and intrawell modes as well as manifest various energetically higher components of a mode. Most importantly, the observed resonances between different inter- and intrawell modes demonstrate the richness of the system, while their dependence on various system parameters, e.g., the driving frequency, shows the tunability of the system. The above-mentioned realization of multiple resonances constitutes arguably one of the central results of our investigation, which, to the best of our knowledge, has never been reported in such a setting.

Finally, let us comment on possible future extensions of the present work. Our analysis reveals that a combination of different driving protocols can induce admixtures of excited modes which, in the present case, correspond to admixtures of dipolelike and breathinglike modes. In this direction, it would be a natural next step to find the optimal pulse of the interaction quench protocol in order to induce a perfectly shaped squeezed state. Also, the understanding and prediction of the long-time dynamics imposing an interaction quench on a driven lattice at different transient times is certainly of interest.

ACKNOWLEDGMENTS

The authors thank C. V. Morfonios for fruitful discussions. The authors gratefully acknowledge funding by the Deutsche Forschungsgemeinschaft (DFG) in the framework of SFB 925 ("Light induced dynamics and control of correlated quantum systems").

APPENDIX A: HARMONIC OSCILLATOR—ADMIXTURES OF DIPOLELIKE AND BREATHINGLIKE MODES

In the present Appendix we briefly demonstrate the creation of admixtures of excitations consisting of a dipole and a breathing component in the dynamics of a bosonic ensemble confined in a 1D harmonic oscillator. Let us first comment on the creation of each of the above excited modes separately. It is well known that a quench of the frequency of the harmonic oscillator or of the interatomic repulsive interaction induces a breathing-mode oscillation of the atomic cloud. On the other hand, a sudden displacement or a periodic driving, e.g., shaking, of the harmonic oscillator can induce a dipole mode in the atomic cloud. However, a combination of the above techniques can induce more complicated modes in the dynamics [59] and requires computational methods which can take into account higher orbitals, i.e., correlations. Here, we aim at illuminating this scenario by examining the evolution of an atomic cloud consisting of six bosons initially ($t < 0$) prepared in the ground state of a harmonic oscillator potential. Subsequently ($t > 0$) the cloud is subjected to a periodic driving and a simultaneous quench of the interatomic repulsive interaction. Thus, the Hamiltonian that governs the dynamics reads

$$H = \sum_{i=1}^{N} \left(\frac{p_i^2}{2M} + V_D(x_i;t) \right) + g_f \sum_{i<j} \delta(x_i - x_j), \quad \text{(A1)}$$

where the periodic driving of the harmonic oscillator is modeled via the time-dependent potential $V_D(x;t) = \frac{\omega^2}{2}(x - A\sin(\omega_D t))^2$ and $\delta g = g_f - g_{in}$ denotes the quench amplitude. Figure 9(a) illustrates the dynamics of the atomic cloud on the single-particle level by employing the one-body density. It is observed that the cloud not only oscillates inside the external trap but also changes its shape during the oscillation. This is a clear signature that the induced mode is different from a pure dipole mode or a pure breathing mode but it is an admixture of the above-mentioned excitations. To indicate this fact explicitly we illustrate in Fig. 9(b) the profiles of the one-body density at certain instants in time during the evolution. The cloud compresses and decompresses (caused by the interaction quench) during its oscillation (caused by the driven oscillator) inside the external harmonic trap. On the contrary, a cloud which is only subjected to the above

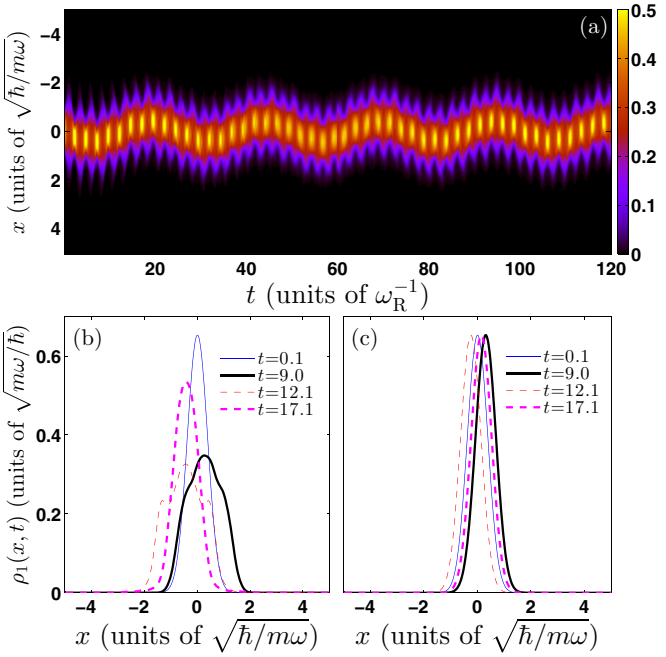

FIG. 9. (a) Time evolution of the one-body density $\rho_1(x,t)$ caused by a periodically driven harmonic trap with $\omega_D = 0.25$ and a simultaneous interaction quench with amplitude $\delta g = 1.6$. The driving amplitude is fixed toat the value $A = 0.6$, while the initial state corresponds to the ground state of six weakly interacting bosons with $g = 0.05$. We also illustrate the one-body density profiles at certain instants in time (see legend) during the evolution of the periodically driven oscillator with (b) $\delta g = 1.6$ and (c) $\delta g = 0$.

external driving [see Fig. 9(c)] performs the well-known dipole oscillation and the wave packet exhibits oscillations with a constant width and amplitude.

APPENDIX B: REMARKS ON THE RESONANT INTRAWELL DYNAMICS OF THE DRIVEN LATTICE

In the present Appendix we briefly comment on the characteristics of the resonant dynamics of the driven lattice from a one-body perspective. Indeed, Fig. 10(a) presents $\rho_1(x,t)$ at $\omega_D = 2.75$. The overall dynamics exhibits enhanced density modulations being manifest as internal fast oscillations and high-amplitude oscillations in each well of period $\sim$20. The interwell tunneling is also enhanced in comparison to that at small ω_D's [see Fig. 2(a)]. A similar intrawell resonant behavior was observed in Ref. [35], where enhanced and in-phase oscillating dipoles were revealed. On the contrary, here, we observe enhanced and out-of-phase oscillating dipole modes as well as an amplified breathing mode in the center. Thus, exploiting the presently used driving scheme we have the possibility of opening an additional energetic channel. To quantify that the driven lattice induced dynamical features are independent of the interaction strength g or the particle number N, we calculate the deviation of the local density oscillation from its mean value, i.e., $\Lambda = \int_0^T dt|\Delta\rho_\alpha(t) - \overline{\Delta\rho_\alpha}|/T$, where $\overline{\Delta\rho_\alpha} = \int_0^T dt\,\Delta\rho_\alpha(t)/T$ denotes the mean oscillation amplitude over the considered propagation time T and $\Delta\rho_\alpha(t)$ refers to the intrawell wave-packet asymmetry. Figure 10(b)

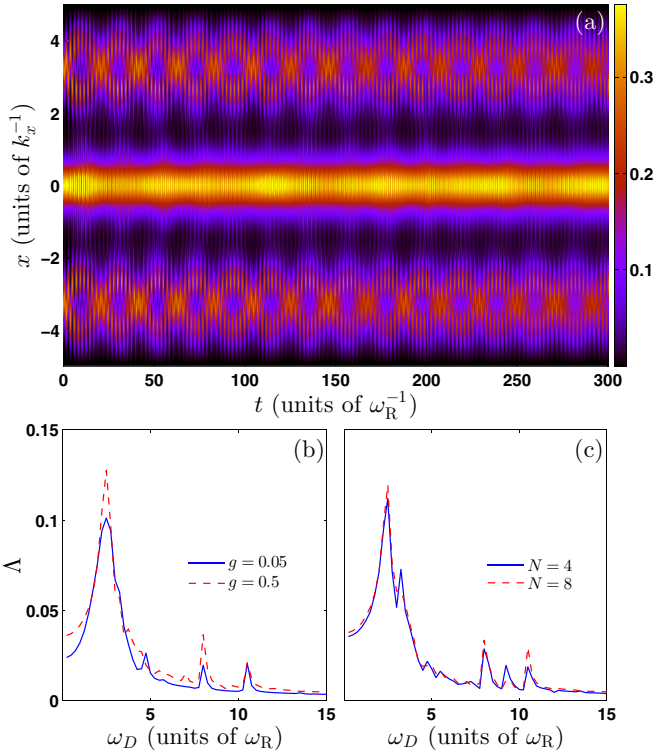

FIG. 10. (a) Time evolution of the one-body density $\rho_1(x,t)$ in a triple well for $\omega_D = 2.75$. The driving amplitude is fixed at the value $\delta = 0.03$, while the initial state corresponds to the ground state of four weakly interacting bosons with $g = 0.05$. (b) Mean oscillation amplitude Λ of the left well for $N = 4$ bosons as a function of the driving frequency ω_D for different interparticle repulsions (see legend). (c) The same as (b), but for fixed interaction $g = 0.2$ and different particle numbers (see legend).

shows the mean amplitude of the intrawell oscillation for the left well as a function of the driving frequency ω_D for different interaction strengths g but the same particle number. The mean amplitude with a varying ω_D increases up to $\omega_D = 2.875$, where it exhibits a peak (position of the resonance) and then decreases again, exhibiting several smaller peaks at frequencies where the system is driven far from equilibrium [see also Fig. 1(a)]. Comparing the dynamics for different interactions it is observed that the ensemble exhibits the same overall behavior but the mean oscillation amplitude is slightly higher (for higher interactions), especially in the region of the central peak. This is a direct interaction effect, since the system possesses more energy. On the other hand, in order to investigate whether the above results are independent of the particle number the same quantity (Λ) is shown in Fig. 10(c) for varying particle numbers, namely, $N = 4$ and 8. The mean amplitude presents the same overall behavior with respect to the driving frequency ω_D but it is also slightly larger for increasing particle number, with a maximal deviation of the order of 30%.

APPENDIX C: THE COMPUTATIONAL APPROACH—MULTICONFIGURATION TIME-DEPENDENT HARTREE METHOD FOR BOSONS

To solve the many-body Schrödinger equation $(i\hbar\partial_t - H)\Psi(x,t) = 0$ of the interacting bosons as an

initial value problem $|\Psi(0)\rangle = |\Psi_0\rangle$, we employ the MCTDHB [39,40,60]. The latter constitutes an efficient and accurate method for both the stationary properties and the nonequilibrium quantum dynamics of systems consisting of a single bosonic species and has already been applied for a wide set of problems (see, e.g., [60–63]). The wave function is represented by a set of variationally optimized time-dependent orbitals, which implies an optimal truncation of the Hilbert space by employing a time-dependent moving basis where the system can be instantaneously optimally represented by time-dependent permanents. Thus, the many-body wave function, which is expanded in terms of the bosonic number states $|n_1,n_2,\ldots,n_M;t\rangle$, based on time-dependent single-particle functions (SPFs) $|\phi_i(t)\rangle$, $i = 1,2,\ldots,M$, reads

$$|\Psi(t)\rangle = \sum_{\vec{n}} C_{\vec{n}}(t)|n_1,n_2,\ldots,n_M;t\rangle. \tag{C1}$$

Here M is the number of SPFs and the summation $\vec{n}$ is over all the possible combinations n_i such that the total number of bosons N is conserved. Note that in the limit in which M approaches the number of grid points the above expansion is equivalent to a full configuration interaction approach. However, in the case of $M = 1$ the many-body wave function is given by a single permanent $|n_1 = N;t\rangle$ and the method reduces to the time-dependent Gross-Pitevskii equation. To determine the time-dependent wave function $|\Psi(t)\rangle$ we need the equations of motion for the coefficients $C_{\vec{n}}(t)$ and the SPFs $|\phi_i(t)\rangle$. Following, e.g., the Dirac-Frenkel [64,65] variational principle, i.e., $\langle\delta\Psi|i\partial_t - \hat{H}|\Psi\rangle = 0$, we end up with the well-known MCTDHB equations of motion [39,40,60], consisting of a set of M nonlinear integrodifferential equations of motion for the orbitals which are coupled to the $\frac{(N+M-1)!}{N!(M-1)!}$ linear equations of motion for the coefficients. Finally, let us remark that in terms of our implementation we use an extended version of the MCTDHB referred to in the literature as the multilayer multi-configuration time-dependent Hartree method for bosons (ML-MCTDHB) [66,67]. This package is particularly suitable for treating systems consisting of different bosonic species, while for the case of a single species it reduces to the MCTDHB.

For our numerical implementation a discrete variable representation for the SPFs and a sine–discrete variable representation, which intrinsically introduces hard-wall boundaries at both edges of the potential, have been employed. The preparation of the initial state has been performed by using the so-called relaxation method in terms of which one obtains the lowest eigenstates of the corresponding m-well setup. The key idea is to propagate some trial wave function $\Psi^{(0)}(x)$ by the nonunitary operator $e^{-H\tau}$. This is equivalent to an imaginary time propagation, and for $\tau \to \infty$ the propagation converges to the ground state, as all other contributions (i.e., $e^{-E_n\tau}$) are exponentially suppressed. In turn, we periodically drive the optical lattice and perform a quench of the strength of the interparticle repulsion and study the evolution of $\Psi(x_1,x_2,\ldots,x_N;t)$ in the m-well potential within the MCTDHB.

Within our simulations the overlap criteria $|\langle\Psi|\Psi\rangle - 1| < 10^{-9}$ and $|\langle\varphi_i|\varphi_j\rangle - \delta_{ij}| < 10^{-10}$ are fulfilled for the total wave function and the SPFs, respectively. Furthermore, to ensure the convergence of our simulations we have used up to 12 (11) optimized SPFs for the triple (11) well, thereby observing

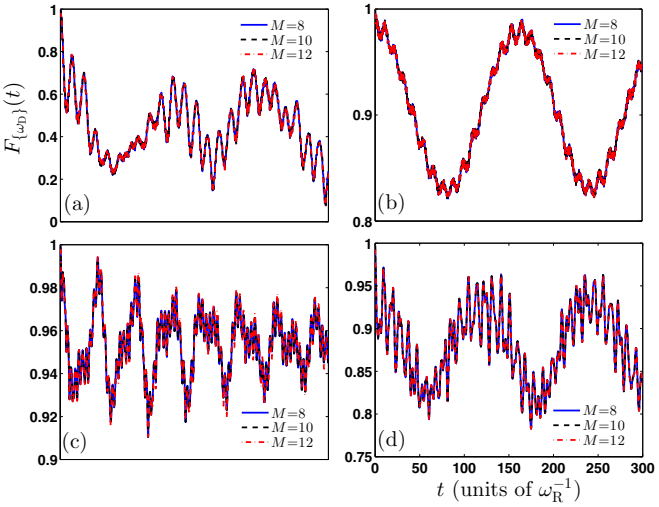

FIG. 11. Fidelity evolution $F_{\omega_D}(t)$ of a periodically driven triple well with (a) $\omega_D = 2.5$ and (b) $\omega_D = 7.5$ with an increasing number of SPFs (see legend). (c), (d) $F_{\omega_D}(t)$ for various SPFs (see legend) with a simultaneous interaction quench of amplitude (c) $\delta g = 0.5$ and (d) $\delta g = 2.0$ on top of the periodically driven triple well with $\omega_D = 0.75$.

a systematic convergence of our results for sufficiently large spatial grids. In particular, we have used 350 spatial grid points in the case of the triple well and 800 spatial grid points for the 11-well potential. In the following, let us briefly demonstrate the convergence procedure concerning our simulations either with an increasing number of SPFs (and a fixed number of 350 grid points) or with a varying number of grid points and a fixed number of SPFs, $M = 12$. Figure 11 shows the fidelity evolution for different numbers of SPFs, namely, $M = 8$, 10, and 12, for the driven triple well at driving frequencies

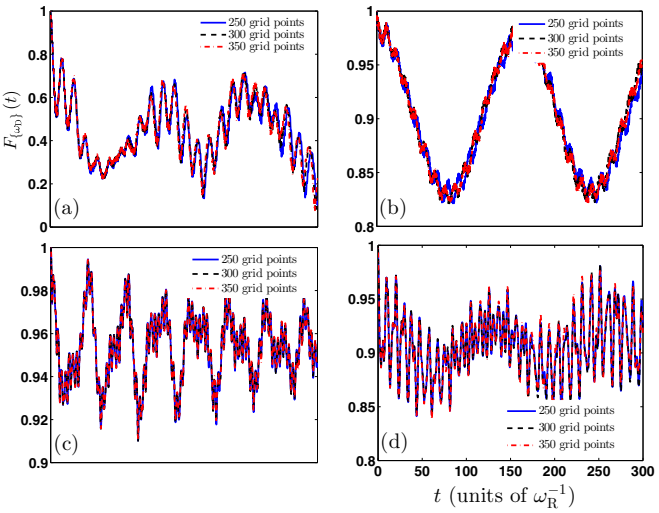

FIG. 12. Fidelity evolution $F_{\omega_D}(t)$ of a periodically driven triple well with (a) $\omega_D = 2.5$ and (b) $\omega_D = 7.5$ with an increasing number of grid sizes (see legend). (c), (d) $F_{\omega_D}(t)$ for various grid sizes (see legend) with a simultaneous interaction quench of amplitude (c) $\delta g = 0.5$ and (d) $\delta g = 2.0$ on top of the periodically driven triple well with $\omega_D = 0.75$.

$\omega_D = 2.5$, $\omega_D = 7.5$ [see Figs. 11(a) and 11(b), respectively], and $F_{\omega_D}(t)$ by employing simultaneous interaction quenches with amplitudes $\delta g = 0.5$, $\delta g = 2.0$ on top of the driving, $\omega_D = 0.75$ [see Figs. 11(c) and 11(d), respectively]. A systematic convergence of the fidelity evolution (for $M > 8$) is observed for increasing numbers of SPFs. For instance, the maximum deviation (at $\omega_D = 2.5$) observed in the fidelity evolution [see Fig. 11(a)] calculated using 8 and 12 SPFs, respectively, is of the order of 0.3% at large evolution times ($t > 200$). Furthermore, in order to show the convergence with an increasing number of grid points Fig. 12 presents the fidelity evolution of the driven triple well at $\omega_D = 2.5$ and $\omega_D = 7.5$ [see Figs. 12(a) and 12(b), respectively] and by performing interaction quenches with $\delta g = 0.5$ and $\delta g = 2.0$ on top of the driven triple well, $\omega_D = 0.75$ [see Figs. 12(c) and 12(d), respectively]. Again, we observe convergence for an increasing number of grid points (especially for grid sizes that contain more than 300 spatial grid points). For instance, the maximum deviation (at $\omega_D = 2.5$) observed in the fidelity evolution [see Fig. 12(a)] calculated using 300 and 350 grid points, respectively (and 12 SPFs), is of the order of 0.1% at large evolution times ($t > 250$). The same analysis was also performed for the 11-well case (omitted here for brevity) showing the same behavior. Another criterion that confirms the achieved convergence is the population of the lowest-occupied natural orbital, kept in each case below 0.1%.

[1] N. Goldman and J. Dalibard, Phys. Rev. X **4**, 031027 (2014).
[2] N. Goldman, J. Dalibard, M. Aidelsburger, and N. R. Cooper, Phys. Rev. A **91**, 033632 (2015).
[3] O. Morsch and M. Oberthaler, Rev. Mod. Phys. **78**, 179 (2006).
[4] I. Bloch, J. Dalibard, and W. Zwerger, Rev. Mod. Phys. **80**, 885 (2008).
[5] A. Polkovnikov, K. Sengupta, A. Silva, and M. Vengalattore, Rev. Mod. Phys. **83**, 863 (2011).
[6] M. Ben Dahan, E. Peik, J. Reichel, Y. Castin, and C. Salomon, Phys. Rev. Lett. **76**, 4508 (1996).
[7] O. Morsch, J. H. Müller, M. Cristiani, D. Ciampini, and E. Arimondo, Phys. Rev. Lett. **87**, 140402 (2001).
[8] T. Hartmann, F. Keck, H. J. Korsch, and S. Mossmann, New J. Phys. **6**, 2 (2004).
[9] A. Eckardt, C. Weiss, and M. Holthaus, Phys. Rev. Lett. **95**, 260404 (2005).
[10] W. Zheng and H. Zhai, Phys. Rev. A **89**, 061603 (2014).
[11] J. Struck, C. Ölschläger, M. Weinberg, P. Hauke, J. Simonet, A. Eckardt, M. Lewenstein, K. Sengstock, and P. Windpassinger, Phys. Rev. Lett. **108**, 225304 (2012).
[12] C. V. Parker, L. C. Ha, and C. Chin, Nat. Phys. **9**, 769 (2013).
[13] S. Choudhury and E. J. Mueller, Phys. Rev. A **90**, 013621 (2014).
[14] P. I. Schneider and A. Saenz, Phys. Rev. A **85**, 050304 (2012).
[15] M. Cheneau, P. Barmettler, D. Poletti, M. Endres, P. Schau, T. Fukuhara, C. Gross, I. Bloch, C. Kollath, and S. Kuhr, Nature **481**, 484 (2012).
[16] S. S. Natu and E. J. Mueller, Phys. Rev. A **87**, 053607 (2013).
[17] W. H. Zurek, U. Dorner, and P. Zoller, Phys. Rev. Lett. **95**, 105701 (2005).
[18] D. Chen, M. White, C. Borries, and B. DeMarco, Phys. Rev. Lett. **106**, 235304 (2011).
[19] M. Rigol, V. Dunjko, and M. Olshanii, Nature **452**, 854 (2008).
[20] E. Altman and A. Auerbach, Phys. Rev. Lett. **89**, 250404 (2002).
[21] W. Kohn, Phys. Rev. **123**, 1242 (1961).
[22] M. Bonitz, K. Balzer, and R. van Leeuwen, Phys. Rev. B **76**, 045341 (2007).
[23] J. W. Abraham and M. Bonitz, Contrib. Plasma Phys. **54**, 27 (2014).
[24] S. Bauch, K. Balzer, C. Henning, and M. Bonitz, Phys. Rev. B **80**, 054515 (2009).
[25] J. W. Abraham, K. Balzer, D. Hochstuhl, and M. Bonitz, Phys. Rev. B **86**, 125112 (2012).
[26] R. Schmitz, S. Krönke, L. Cao, and P. Schmelcher, Phys. Rev. A **88**, 043601 (2013).
[27] S. Peotta, D. Rossini, M. Polini, F. Minardi, and R. Fazio, Phys. Rev. Lett. **110**, 015302 (2013).
[28] H. Lignier, C. Sias, D. Ciampini, Y. Singh, A. Zenesini, O. Morsch, and E. Arimondo, Phys. Rev. Lett. **99**, 220403 (2007).
[29] C. Sias, H. Lignier, Y. P. Singh, A. Zenesini, D. Ciampini, O. Morsch, and E. Arimondo, Phys. Rev. Lett. **100**, 040404 (2008).
[30] E. Haller, R. Hart, M. J. Mark, J. G. Danzl, L. Reichsöllner, and H. C. Nägerl, Phys. Rev. Lett. **104**, 200403 (2010).
[31] Y.-A. Chen, S. Nascimbène, M. Aidelsburger, M. Atala, S. Trotzky, and I. Bloch, Phys. Rev. Lett. **107**, 210405 (2011).
[32] S. Rosi, A. Bernard, N. Fabbri, L. Fallani, C. Fort, M. Inguscio, T. Calarco, and S. Montangero, Phys. Rev. A **88**, 021601 (2013).
[33] C. Brif, R. Chakrabarti, and H. Rabitz, in *Advances in Chemical Physics*, edited by S. A. Rice and A. R. Dinner (Wiley, New York, 2012), Vol. 148, pp. 1–76.
[34] C. Brif, R. Chakrabarti, and H. Rabitz, New J. Phys. **12**, 075008 (2010).
[35] S. I. Mistakidis, T. Wulf, A. Negretti, and P. Schmelcher, J. Phys. B **48**, 244004 (2015).
[36] S. I. Mistakidis, L. Cao, and P. Schmelcher, J. Phys. B **47**, 225303 (2014).
[37] S. I. Mistakidis, L. Cao, and P. Schmelcher, Phys. Rev. A **91**, 033611 (2015).
[38] S. Fölling, S. Trotzky, P. Cheinet, M. Feld, R. Saers, A. Widera, T. Müller, and I. Bloch, Nature (London) **448**, 1029 (2007).
[39] O. E. Alon, A. I. Streltsov, and L. S. Cederbaum, J. Chem. Phys. **127**, 154103 (2007).
[40] O. E. Alon, A. I. Streltsov, and L. S. Cederbaum, Phys. Rev. A **77**, 033613 (2008).
[41] M. Olshanii, Phys. Rev. Lett. **81**, 938 (1998).
[42] T. Köhler, K. Goral, and P. S. Julienne, Rev. Mod. Phys. **78**, 1311 (2006).
[43] C. Chin, R. Grimm, P. Julienne, and E. Tiesinga, Rev. Mod. Phys. **82**, 1225 (2010).
[44] J. I. Kim, V. S. Melezhik, and P. Schmelcher, Phys. Rev. Lett. **97**, 193203 (2006).
[45] P. Giannakeas, F. K. Diakonos, and P. Schmelcher, Phys. Rev. A **86**, 042703 (2012).
[46] P. Giannakeas, V. S. Melezhik, and P. Schmelcher, Phys. Rev. Lett. **111**, 183201 (2013).

[47] S. Klaiman and O. E. Alon, Phys. Rev. A **91**, 063613 (2015).
[48] S. Klaiman, A. I. Streltsov, and O. E. Alon, Phys. Rev. A **93**, 023605 (2016).
[49] J. P. Ronzheimer, M. Schreiber, S. Braun, S. S. Hodgman, S. Langer, I. P. McCulloch, F. Heidrich-Meisner, I. Bloch, and U. Schneider, Phys. Rev. Lett. **110**, 205301 (2013).
[50] U. M. Titulaer and R. J. Glauber, Phys. Rev. **140**, B676 (1965).
[51] M. Naraschewski and R. J. Glauber, Phys. Rev. A **59**, 4595 (1999).
[52] K. Sakmann, A. I. Streltsov, O. E. Alon, and L. S. Cederbaum, Phys. Rev. A **78**, 023615 (2008).
[53] R. W. Spekkens and J. E. Sipe, Phys. Rev. A **59**, 3868 (1999).
[54] S. Klaiman, N. Moiseyev, and L. S. Cederbaum, Phys. Rev. A **73**, 013622 (2006).
[55] E. J. Mueller, T. L. Ho, M. Ueda, and G. Baym, Phys. Rev. A **74**, 033612 (2006).
[56] K. Sakmann, A. I. Streltsov, O. E. Alon, and L. S. Cederbaum, Phys. Rev. A **89**, 023602 (2014).
[57] O. Penrose and L. Onsager, Phys. Rev. **104**, 576 (1956).
[58] I. Brouzos, S. Zöllner, and P. Schmelcher, Phys. Rev. A **81**, 053613 (2010).
[59] O. I. Streltsova, O. E. Alon, L. S. Cederbaum, and A. I. Streltsov, Phys. Rev. A **89**, 061602 (2014).
[60] A. I. Streltsov, O. E. Alon, and L. S. Cederbaum, Phys. Rev. Lett. **99**, 030402 (2007).
[61] A. I. Streltsov, K. Sakmann, O. E. Alon, and L. S. Cederbaum, Phys. Rev. A **83**, 043604 (2011).
[62] O. E. Alon, A. I. Streltsov, and L. S. Cederbaum, Phys. Rev. A **76**, 013611 (2007).
[63] O. E. Alon, A. I. Streltsov, and L. S. Cederbaum, Phys. Rev. A **79**, 022503 (2009).
[64] J. Frenkel, *Wave Mechanics*, 1st ed. (Clarendon Press, Oxford, UK, 1934), pp. 423–428.
[65] P. A. Dirac, Proc. Cambridge Philos. Soc. **26**, 376 (1930).
[66] L. Cao, S. Krönke, O. Vendrell, and P. Schmelcher, J. Chem. Phys. **139**, 134103 (2013).
[67] S. Krönke, L. Cao, O. Vendrell, and P. Schmelcher, New J. Phys. **15**, 063018 (2013).